JCI The Journal of Clinical Investigation

Peroxisome-derived lipids regulate adipose thermogenesis by mediating cold-induced mitochondrial fission

Hongsuk Park, … , Katsuhiko Funai, Irfan J. Lodhi

J Clin Invest. 2018. https://doi.org/10.1172/JCI120606.

Research In-Press Preview **Cell biology** **Metabolism**

Peroxisomes perform essential functions in lipid metabolism, including fatty acid oxidation and plasmalogen synthesis. Here, we describe a role for peroxisomal lipid metabolism in mitochondrial dynamics in brown and beige adipocytes. Adipose tissue peroxisomal biogenesis was induced in response to cold exposure through activation of the thermogenic co-regulator PRDM16. Adipose-specific knockout of the peroxisomal biogenesis factor Pex16 (*Pex16-AKO*) in mice impaired cold tolerance, decreased energy expenditure, and increased diet-induced obesity. Pex16 deficiency blocked cold-induced mitochondrial fission, decreased mitochondrial copy number, and caused mitochondrial dysfunction. Adipose-specific knockout of the peroxisomal beta-oxidation enzyme acyl CoA oxidase 1 (*Acox1-AKO*) was not sufficient to affect adiposity, thermogenesis or mitochondrial copy number, but knockdown of the plasmalogen synthetic enzyme glyceronephosphate O-acyltransferase (GNPAT) recapitulated the effects of Pex16 inactivation on mitochondrial morphology and function. Plasmalogens are present in mitochondria and decreased with Pex16 inactivation. Their dietary supplementation increased mitochondrial copy number, improved mitochondrial function, and rescued thermogenesis in *Pex16-AKO* mice. These findings support a surprising interaction between peroxisomes and mitochondria to regulate mitochondrial dynamics and thermogenesis.

Find the latest version:

https://jci.me/120606/pdf

Peroxisome-derived lipids regulate adipose thermogenesis by mediating cold-induced mitochondrial fission

Hongsuk Park[1*], Anyuan He[1*], Min Tan[1], Jordan M. Johnson[2], John M. Dean[1], Terri A. Pietka[3], Yali Chen[1], Xiangyu Zhang[4], Fong-Fu Hsu[1], Babak Razani[4,5], Katsuhiko Funai[2], and Irfan J. Lodhi[1#]

[1]Division of Endocrinology, Metabolism and Lipid Research; Department of Medicine, Washington University School of Medicine, Saint Louis, MO 63110, USA
[2]Diabetes & Metabolism Research Center, University of Utah, Salt Lake City, UT 84112, USA
[3]Nutrition and Geriatrics Division, Department of Medicine, Washington University School of Medicine, Saint Louis, MO 63110, USA
[4]Cardiology Division, Department of Medicine, Washington University School of Medicine, Saint Louis, MO 63110, USA
[5]Veterans Affairs St. Louis Healthcare System, John Cochran Division, Saint Louis, MO 63106, USA

[*]H.P. and A.H. contributed equally to this work.

[#]Contact:
Irfan J. Lodhi
Washington University School of Medicine
660 S. Euclid Avenue, Campus Box 8127
Saint Louis, MO 63110
Tel: 314-747-6766
Email: ilodhi@wustl.edu

Abstract

Peroxisomes perform essential functions in lipid metabolism, including fatty acid oxidation and plasmalogen synthesis. Here, we describe a role for peroxisomal lipid metabolism in mitochondrial dynamics in brown and beige adipocytes. Adipose tissue peroxisomal biogenesis was induced in response to cold exposure through activation of the thermogenic co-regulator PRDM16. Adipose-specific knockout of the peroxisomal biogenesis factor Pex16 (*Pex16-AKO*) in mice impaired cold tolerance, decreased energy expenditure, and increased diet-induced obesity. Pex16 deficiency blocked cold-induced mitochondrial fission, decreased mitochondrial copy number, and caused mitochondrial dysfunction. Adipose-specific knockout of the peroxisomal β-oxidation enzyme acyl CoA oxidase 1 (*Acox1-AKO*) was not sufficient to affect adiposity, thermogenesis or mitochondrial copy number, but knockdown of the plasmalogen synthetic enzyme glyceronephosphate O-acyltransferase (GNPAT) recapitulated the effects of Pex16 inactivation on mitochondrial morphology and function. Plasmalogens are present in mitochondria and decreased with Pex16 inactivation. Their dietary supplementation increased mitochondrial copy number, improved mitochondrial function, and rescued thermogenesis in *Pex16-AKO* mice. These findings support a surprising interaction between peroxisomes and mitochondria to regulate mitochondrial dynamics and thermogenesis.

Introduction

Obesity remains a serious global health problem that increases the risk for type 2 diabetes and other diseases, including cardiovascular disease and several forms of cancer. Current pharmacological approaches to treat obesity primarily target energy intake by suppressing appetite or blocking intestinal absorption of fat and are associated with multiple side effects, suggesting a need for alternative approaches. Targeting brown adipose tissue (BAT) function to increase energy expenditure represents one such approach. Unlike white adipose tissue (WAT), which is involved in storing excess energy as fat that can be mobilized in times of need, BAT oxidizes chemical energy in food to generate heat through uncoupled respiration in response to beta adrenergic stimulation. In addition to the classical BAT, brown adipocyte-like beige cells appear within subcutaneous WAT in response to prolonged cold exposure. Brown and beige fat are enriched in mitochondria and express uncoupling protein 1 (UCP1), a mitochondrial membrane protein that uncouples respiration from ATP synthesis. Because thermogenesis promotes energy expenditure, increasing the activity of brown and beige fat cells may be an attractive strategy for treating obesity.

Like mitochondria, peroxisomes are abundantly present in BAT (1). As multifunctional organelles, peroxisomes are involved in a variety of metabolic functions, including β-oxidation of very long chain fatty acids (VLCFAs), α-oxidation of methyl-branched fatty acids, synthesis of ether lipids and bile acids, and production and decomposition of reactive oxygen species (ROS) (2).

Peroxisomes are generated through growth and division of existing peroxisomes or through de novo peroxisomal biogenesis. Recent studies suggest that de novo formation of peroxisomes requires fusion of a pre-peroxisomal vesicle derived from the ER with a vesicle derived from the mitochondria (3). Assembly of functional peroxisomes involves proteins called peroxins that are required for various aspects of peroxisomal biogenesis (4). Mutations in these factors result in peroxisomal biogenesis disorders in the Zellweger spectrum, devastating conditions characterized by a host of abnormalities (5). Three of these factors (Pex3, Pex16, and Pex19) are critical for assembly of the peroxisomal membrane and import of peroxisomal membrane proteins (PMPs). Humans with null mutations of these peroxins lack peroxisomes. Pex19 is a chaperone and import receptor for newly synthesized PMPs (6). Pex16 buds from the ER in a pre-peroxisomal vesicle and fuses with a pre-peroxisomal vesicle containing Pex3 (and Pex14) at the mitochondrial surface, resulting in a peroxisome that can import its matrix proteins and proliferate through growth and division (3). Peroxisomal matrix proteins are translated on free ribosomes in the cytoplasm prior to their import. These proteins have specific peroxisomal targeting sequences (PTS) located either at the carboxyl (PTS1) or amino (PTS2) terminus (7, 8). The import receptor for PTS1-containing peroxisomal matrix proteins is Pex5 (9). PTS2-containing peroxisomal matrix proteins require Pex7 for their import into the peroxisome (10).

Cold exposure has been shown to increase peroxisomes and their enzyme activities in BAT (11-13). However, the physiological significance of peroxisomes in BAT is poorly understood. Efforts to understand the role of peroxisomes in adipose tissue using mice with knockout of *Pex5* driven by *aP2-Cre* were impeded by the non-specificity of the Cre driver, which deleted the gene in multiple other tissues besides adipose tissue, including the brain and the peripheral nervous

system, resulting in a complicated phenotype related to compromised muscle function (14). Thus, whether peroxisomes are required for BAT-mediated (non-shivering) thermogenesis and the mechanism through which they might regulate this process remain unknown.

Using a new model of adipose-specific peroxisome deficiency generated through *adiponectin-Cre*-mediated knockout of *Pex16,* here we demonstrate that peroxisomes are critical for adipose tissue thermogenesis. Mechanistically, our results uncover a previously unrecognized role for peroxisomes in division of mitochondria in brown and beige adipocytes.

Results

Peroxisomal biogenesis increases in adipose tissue in response to cold exposure and high fat feeding. The physiological role of peroxisomes in adipose tissue remains unclear. Thus, we assessed peroxisomal biogenesis genes during differentiation of primary brown and white adipocytes (Supplemental Figure 1). Quantitative real-time PCR analysis showed induction of genes involved in peroxisomal biogenesis during both brown and white adipogenesis, with more dramatic increases during brown adipogenesis. aP2, a known marker of adipogenesis was increased, as expected (Supplemental Figure 1A). We also compared the expression of genes encoding various peroxisomal proteins in BAT or gonadal WAT (gWAT) in mice fed normal chow diet or a HFD (Supplemental Figure 1B). Peroxisomal genes were generally expressed more highly in BAT as compared to WAT and further increased in BAT, but not WAT, with high fat feeding (Supplemental Figure 1B). Western blot analysis confirmed the HFD-induced increased expression in BAT (Supplemental Figure 1C). This suggests that peroxisomes are particularly important in brown fat function.

To understand the role of peroxisomes in adipose tissue thermogenesis, we performed gene expression analysis on BAT, inguinal WAT (iWAT) and gWAT from mice kept at room temperature (22^{o}C) or subjected to cold exposure (4^{o}C) (Figure 1). Cold exposure increased the expression of genes involved in peroxisomal biogenesis in BAT, as well as in iWAT, which is highly susceptible to cold-induced browning (15), but not in gWAT (Figure 1A). These data suggest that peroxisomes in brown and beige adipocytes are involved in thermogenesis.

PRDM16 regulates cold-induced peroxisomal biogenesis. Adipose tissue-mediated thermogenesis requires PRDM16, a large zinc finger containing transcription factor that regulates gene expression by interacting with and modulating the activity of other transcription factors, including C/EBPβ, PGC1α, PPARα and PPARγ (15). Microarray analysis identified Pex16 as a potential transcriptional target of PRDM16 (16). Thus, we sought to determine whether PRDM16 might be involved in peroxisomal biogenesis. To examine if PRDM16 regulates Pex16 expression, we created a GFP reporter construct under the control of a -2kb mouse Pex16 promoter. Overexpression of PRDM16 in Cos-7 cells increased GFP expression (Figure 1B). To quantify the effect of PRDM16 on the Pex16 promoter, we also generated a luciferase reporter plasmid. Overexpression of PRDM16 increased the expression of luciferase under the control of Pex16 promoter (Figure 1C). To determine if PRDM16 directly regulates Pex16 gene expression, we isolated the stromal vascular fraction (SVF) of BAT from *wild-type C57* mice, infected the cells with retrovirus expressing FLAG-PRDM16, and performed chromatin immunoprecipitation (ChIP) assays using an anti-FLAG antibody followed by qPCR using primers targeting various regions of the Pex16 promoter. PRDM16 interacted with a

proximal region of the Pex16 promoter (Figure 1D). Together, these data strongly suggest that PRDM16 directly regulates the Pex16 expression.

To determine if PRDM16 is required for the expression of other peroxisomal genes and is involved in cold-induced peroxisomal biogenesis, we generated mice with adipose-specific PRDM16 knockout (*PRDM16-AKO*) by crossing *PRDM16*$^{Lox/Lox}$ animals (17) with *adiponectin-Cre* mice (18). We maintained 6-week old *PRDM16-AKO* and control mice at room temperature or subjected them to cold exposure and conducted gene expression analysis in iWAT. Although PRDM16 was dispensable for constitutive peroxisomal biogenesis, its knockout completely blocked cold-induced increase in peroxisomal biogenesis in iWAT, without affecting the expression of genes involved in lysosomal function, such as *Ctsb* and *Lipa* (Figure 1E). In the classical BAT of cold-treated mice, PRDM16 inactivation resulted in only modest (20-30%) reduction in the expression of certain peroxisomal biogenesis genes and even *Ucp1*, a known PRDM16 target gene, was only 40% decreased (Supplemental Figure 1D), consistent with previous studies suggesting that a related transcription factor PRDM3 can compensate for the loss of PRDM16 in BAT, particularly in younger mice (19).

Generation of adipose-specific Pex16 knockout mice. Pex16 is required for peroxisomal biogenesis (20). Immunofluorescence analysis in differentiated BAT SVF cells demonstrated a strong co-localization of Pex16 with PMP70, a peroxisomal marker and, not with COX IV, a mitochondrial marker (Supplemental Figure 2). To study the role of peroxisomes in thermogenesis, we generated *Pex16*$^{Lox/Lox}$ mice (Figure 2) and crossed them with *adiponectin-Cre* to create adipose-specific Pex16 KO (*Pex16-AKO*) mice (Figure 2A). The mutant mice were

born at the expected Mendelian frequency and were overtly normal. Rearrangement at the Pex16 locus was confirmed by PCR (Figure 2B), and Pex16 expression was decreased in gWAT, iWAT and BAT, but not the liver (Figure 2C). Although there was no effect on the mRNA expression of other peroxisomal genes, including *Pex7* and *Pmp70* (Figure 2D), immunofluorescence analysis using an antibody against PMP70 indicated that *Pex16-AKO* mice lack peroxisomes in BAT (Figure 2E). Western blot analysis in iWAT confirmed the knockout of Pex16 and indicated that other peroxisomal proteins are degraded in the absence of peroxisomes (Figure 2F). Together, these data demonstrate that Pex16 is critical for peroxisomal biogenesis in adipose tissue.

Mice with adipose-specific knockout of Pex16 have increased diet-induced obesity and impaired thermogenesis. To determine the effect on adiposity and metabolism, we phenotypically characterized the mice (Figure 3). In the mice fed normal chow diet, no significant difference in body weight between the genotypes was observed (Figure 3A). High fat feeding resulted in late-onset obesity in *Pex16-AKO* mice (Figure 3B), a phenotype resembling animals with adipose-specific knockout of PRDM16 (17). Interestingly, this effect of high fat feeding was only seen in the mice housed at room temperature (22^{o}C), which is a mild cold challenge for mice that achieve thermoneutrality at approximately 30^{o}C (21). At thermoneutrality, control and *Pex16-AKO* mice weighed the same (Figure 3C), suggesting that the increased diet-induced obesity in the room temperature-housed knockout mice likely reflects impaired thermogenesis.

Body composition analysis performed in room temperature-kept mice after 20 weeks on HFD, when the weight curves had begun to diverge, indicated that the knockout mice had significantly increased adiposity (Figure 3D). The gWAT depot weighed significantly more in the knockout (Figure 3E), while chow-fed animals had no phenotypic differences (Supplemental Figure 3, A and B). Histologic analysis indicated that white adipocytes were larger in HFD-fed knockout animals (Figure 3F; Supplemental Figure 3, C and D). The increased adiposity was observed despite the fact that there was no difference in food intake (Supplemental Figure 3E) or physical activity (Supplemental Figure 3F). Assessment of glucose homeostasis indicated that although glucose tolerance was significantly impaired in chow-fed *Pex16-AKO* mice (Supplemental Figure 3G), the difference between the genotypes was lost in animals fed HFD for 14 weeks (Supplemental Figure 3H).

We next determined the effect of Pex16 inactivation on energy expenditure and thermogenesis. Indirect calorimetry performed in mice fed HFD for 15 weeks at 22^{o}C indicated that there was no difference in resting energy metabolism (Supplemental Figure 3, I-K), consistent with previous studies suggesting that indirect calorimetry is not sufficiently sensitive to detect subtle changes in energy expenditure that result in modest obesity over an extended period (17, 22). However, the rate of oxygen consumption (VO_2) after treatment of mice with β-adrenergic receptor agonist norepinephrine (NE) was significantly decreased in *Pex16-AKO* mice (Figure 3G), suggesting that BAT function might be impaired. Consistent with this possibility, histologic analysis of BAT indicated there was a marked accumulation of lipids in BAT after cold treatment in the *Pex16-AKO* mice (Figure 3H). BAT from cold-treated knockout animals was pale in appearance (Figure 3I) and had significantly higher triglyceride content (Figure 3J).

To determine if the increased adiposity and elevated accumulation of lipids in BAT were due to impaired thermogenesis, we subjected singly housed mice to acute cold exposure (4^{o}C). *Pex16-AKO* mice were severely cold intolerant (Figure 3K) and succumbed to the cold challenge within 8-40 hrs (Figure 3L). Together, these data suggest that peroxisomes are critical for brown fat-mediated thermogenesis.

Inhibition of peroxisomal biogenesis blocks cold-induced mitochondrial fission and impairs mitochondrial function in brown and beige adipocytes. Since mitochondria are critical for thermogenesis and mitochondrial respiration accounts for most of the cellular oxygen consumption, the impaired thermogenesis and reduced rate of NE-induced oxygen consumption in *Pex16-AKO* mice prompted us to examine the effects of Pex16 inactivation on mitochondrial structure and function in the BAT of mice (Figure 4). Transmission electron microscopic (TEM) analysis indicated that mitochondria in the BAT of control mice at room temperature had an elliptical shape (Figure 4A). Cold exposure resulted in the appearance of circular mitochondria in these mice with an aspect ratio of close to 1 (Figure 4B) and the total number of mitochondria per cell significantly increased (Figure 4C), consistent with previous studies suggesting that β-adrenergic stimulation promotes mitochondrial fission in brown adipocytes (23). Interestingly, this cold-induced mitochondrial division was blocked in the knockout BAT and the mitochondria maintained an elongated morphology. Nevertheless, the mitochondria in the *Pex16-AKO* brown adipocytes appeared to have healthy looking cristae (Figure 4A) and the membrane potential measured using TMRE (tetramethylrhodamine, ethyl ester) dye was also unaffected following Pex16 knockdown in brown adipocytes (Supplemental Figure 4A). TEM analysis also indicated

that lipid droplets were larger in BAT of *Pex16-AKO* mice as compared to control mice (Figure 4A and Supplemental Figure 4B).

Consistent with the possibility that loss of peroxisomes impairs mitochondrial division in BAT, Pex16 knockout significantly decreased mitochondrial DNA copy number in mice at room temperature and completely blocked the cold-induced increase in mitochondrial DNA content (Figure 4D). Pex16 knockout also suppressed the cold-induced increase in mtDNA content in iWAT (Figure 4E), suggesting that similar mechanisms might be at play both in BAT and iWAT. Quantitative real-time PCR analysis in BAT from cold-treated mice indicated that the mitochondrial transcripts *MtCo1* (Cytochrome C Oxidase I), *MtCo2* (Cytochrome C Oxidase II) and *MtNd6* (Mitochondrially-encoded NADH:Ubiquinone Oxidoreductase Core Subunit 6), representing components of the oxidative phosphorylation (OXPHOS) pathway were significantly decreased, while nuclear-encoded genes for mitochondrial proteins (e.g. *Ucp1* and *Cs*) or factors involved in mitochondrial biogenesis (*Tfam* and *Nrf1*) were unaffected (Figure 4F). Western blot analysis confirmed that the expression levels of UCP1 and Cytochrome C Oxidase IV (COX IV), a nuclear-encoded component of the mitochondrial electron transport chain, were unaffected with Pex16 inactivation in BAT (Supplemental Figure 4C).

Mitochondrial division requires dynamin-related protein 1 (Drp1), a cytosolic GTPase that is recruited to the mitochondrial outer membrane during fission (24). Gene expression of *Drp1*, other factors involved in mitochondrial fission (*Fis1* and *Mff*), or factors involved in mitochondrial fusion (*Mfn1*, *Mfn2* and *Opa1*) were unchanged in BAT with Pex16 inactivation (Figure 4F). Moreover, Western blot analysis indicated that the levels of Drp1 were unchanged

in the mitochondrial fractions isolated from BAT of cold-treated control and *Pex16-AKO* mice (Supplemental Figure 4D). This suggests that inhibition of peroxisomal biogenesis in brown adipocytes does not block Drp1 recruitment to mitochondria or its gene expression, but might inhibit its ability to fragment mitochondria.

Cell autonomous effects of Pex16 inactivation on mitochondrial morphology and function. To determine if the effects of Pex16 inactivation on mitochondrial DNA content and morphology were cell autonomous, we treated BAT SVF cells with lentiviral shRNA for Pex16 (Figure 5). Unlike knockdown of Pex16 in undifferentiated 3T3-L1 cells, which has been shown to block PPARγ signaling and adipogenesis (25), knockdown of Pex16 during the late stage of differentiation in BAT SVF cells (Figure 5A) did not decrease adipogenic gene expression or accumulation of lipid droplets (Supplemental Figure 5, A and B). However, this intervention significantly decreased mtDNA (Figure 5B). It is noteworthy that although mitochondria in BAT were fragmented only after cold exposure of mice (Figure 4A), mitochondria in cultured brown adipocytes were constitutively fragmented (Figure 5C), perhaps because cell culture represents a nutrient surplus condition. Under such conditions, mitochondria tend to be more fragmented and exhibit reduced bioenergetic efficiency (26). Pex16 knockdown resulted in elongated mitochondria that formed net-like structures, a characteristic feature of impaired mitochondrial fission as observed with genetic inactivation of *Drp1*(27-29). Treatment of BAT SVF cells with Mdivi-1, a cell-permeable inhibitor of Drp1 (30), also resulted in tubular mitochondria and Pex16 knockdown did not further exacerbate this phenotype (Figure 5C). The mitochondrial morphology was quantified by visual inspection of cells to determine the percentage of cells exhibiting fragmented, fused or intermediate (partially fragmented) mitochondria (Figure 5D).

We next determined if mitochondrial function was altered due to peroxisome deficiency in brown adipocytes. Basal and NE-stimulated oxygen consumption rate (OCR) measured using a Seahorse XF24 Extracellular Flux Analyzer was significantly decreased with Pex16 knockdown (Figure 5E), consistent with the decreased expression of OXPHOS genes (Figure 4F). We also performed high resolution respirometry using an Oroboros Oxygraph-O2k system to assess mitochondrial function in BAT and iWAT from cold-treated control and *Pex16-AKO* mice after sequential additions of different substrates, including octanoyl carnitine (OC); pyruvate (Pyr); glutamate and malate (G+M); and ADP and succinate (ADP+S). There was a trend for the mitochondrial respiration to be decreased in BAT of *Pex16-AKO* mice in response to various substrates, but the effects did not reach statistical significance. However, the maximum respiration after the addition of the mitochondrial uncoupler FCCP was significantly lower in BAT of *Pex16-AKO* mice (Figure 5F**)**. The mitochondrial respiration was significantly lower in iWAT of *Pex16-AKO* mice after addition of various substrates and FCCP (Figure 5G**)**. Together, these data suggest that inhibition of peroxisomal biogenesis impairs cold-induced mitochondrial division, resulting in decreased mtDNA content and disruption of mitochondrial function in brown and beige fat.

BAT-specific Pex16 knockout reduces respiration, but is not sufficient to fully impair thermogenesis. To understand the relative contribution of BAT versus WAT in peroxisome-dependent regulation of thermogenesis, we generated mice with BAT-specific knockout of Pex16 (*Pex16-BKO*) by crossing *Pex16*$^{Lox/Lox}$ with *Ucp1-Cre* transgenic mice (Figure 6). Cre-mediated recombination at the Pex16 locus in BAT was confirmed by PCR (Figure 6A) and

Western blot analysis demonstrated that Pex16 was selectively knocked out in BAT and not in WAT depots (Figure 6B). Gene expression analysis indicated that mitochondrial transcripts *MtCo1*, *MtCo2* and *MtNd6* were significantly decreased in BAT of *Pex16-BKO* mice (Figure 6C). *Cs* was also decreased modestly, but significantly. Indirect calorimetry demonstrated that VO_2 was significantly lower after treatment with NE in the mutant mice (Figure 6D). Nevertheless, the *Pex16-BKO* mice were surprisingly only modestly less cold tolerant as compared to control mice (Figure 6E). This was not because of a compensatory increase in the gene expression of *Ucp1* or genes involved in UCP1-independent mechanisms of thermogenesis, including SERCA2b-dependent Ca^{2+} cycling and creatine metabolism pathways (31, 32) in iWAT (Figure 6F).

Together, these results suggest that peroxisomal biogenesis both in BAT and WAT is required for thermogenesis. Although knockout of Pex16 in BAT alone reduces respiration, it is not sufficient to fully impair thermogenesis.

Pex16 knockout impairs peroxisomal and mitochondrial fatty acid oxidation. Since inhibition of mitochondrial fatty acid oxidation (FAO) has been shown to result in increased accumulation of lipid droplets in BAT and impaired thermogenesis (33), phenotypes resembling our *Pex16-AKO* mice, we sought to determine if mitochondrial and/or peroxisomal FAO pathways were affected due to Pex16 deficiency (Figure 7). Although Pex16 knockout appears to result in degradation of the peroxisomal FAO enzyme acyl CoA oxidase 1 (Acox1) protein (Figure 2F**)**, its gene expression was not decreased, but slightly increased (Figure 7A). Other FAO genes, including those for the peroxisomal enzyme 3-ketoacyl CoA thiolase (*Acaa1*) and the

mitochondrial enzyme carnitine palmitoyltransferase 1 (*Cpt1*), which are thought to be PPARα transcriptional targets, as well as *Ppara* itself, were significantly increased in BAT of *Pex16-AKO* mice (Figure 7A). The gene expression of some FAO enzymes, including peroxisomal multifunctional protein 2 (*Hsd17b4*) and medium-chain acyl-CoA dehydrogenase (*Acadm*), were not significantly affected. The increased expression of certain PPARα target genes is consistent with previous studies suggesting that peroxisomal FAO regulates metabolism of an endogenous ligand of this nuclear receptor (34). Direct measurement of FAO using radiolabeled substrates indicated that oxidation of lignoceric acid (C24:0), a VLCFA that is oxidized exclusively in peroxisomes, as well as oxidation of palmitate (C16:0), which occurs primarily in mitochondria, were significantly blocked with Pex16 knockout (Figures 7, B and C). To determine if the impaired mitochondrial FAO simply reflects a general decrease in mitochondrial function in *Pex16-AKO* mice, we normalized the palmitate oxidation to citrate synthase activity. The citrate synthase activity itself was modestly decreased in BAT of *Pex16-AKO* mice (Supplemental Figure 6A). Palmitate oxidation normalized to this activity was still significantly lower in *Pex16-AKO* mice than control animals (Supplemental Figure 6B).

Inactivation of peroxisomal β-oxidation is not sufficient to impair thermogenesis. Given the impaired oxidation of VLCFAs and degradation of the Acox1 protein, one potential mechanism of the mitochondrial dysfunction and defective thermogenesis in *Pex16-AKO* mice could be that accumulation of these peroxisomal FAO substrates results in mitochondrial toxicity. To explore this possibility, we generated mice with adipose-specific inhibition of Acox1, which catalyzes the first and rate-limiting step in VLCFA oxidation (35). Mice with global knockout of *Acox1* (*Acox1*$^{-/-}$) have a complicated phenotype characterized by growth retardation and hepatocellular

carcinoma (36). Thus, we used the CRISPR/Cas9 system to generate mice with floxed alleles of *Acox1* (Figure 7D). We crossed the *Acox1*$^{Lox/Lox}$ mice with *adiponectin-Cre* mice to generate animals with adipose-specific knockout of *Acox1* (*Acox1-AKO*). Quantitative real-time PCR analysis indicated that the *Acox1* message was significantly decreased, while the expression of genes involved in peroxisomal biogenesis, mitochondrial FAO, and other genes in the peroxisomal FAO pathway were unchanged (Figure 7E). Acox1 knockout also had no effect on the expression of Acox2 and Acox3, which are involved in branched chain fatty acid oxidation and/or bile acid metabolism (37) and are present at much lower levels as compared to Acox1 in BAT and iWAT (Supplemental Figures 7, A and B).

Knockout of Acox1 in BAT and iWAT was confirmed by Western blot analysis (Figure 7F). Inhibition of VLCFA oxidation due to Acox1 inactivation was confirmed by measuring catabolism of stable-isotope labelled docosanoic acid (D_3-C22:0) to D_3-C16:0 via mass spectrometric analysis in control and Acox1-KO iWAT SVF cells (Figure 7G). Surprisingly, adipose-specific inactivation of Acox1 did not affect diet-induced obesity (Figure 7H**),** nor did it impair cold tolerance (Figure 7I) or reduce BAT mitochondrial copy number (Figure 7J). Knockdown of *Acox2* or *Acox3* in BAT SVF cells using lentiviral shRNA (Supplemental Figure 7C) also did not affect mtDNA content (Supplemental Figure 7D). Together, these data suggest that the increased adiposity, impaired thermogenesis and mitochondria dysfunction caused by Pex16 knockout-mediated inhibition of peroxisomal biogenesis in adipose tissue are not likely due to a loss of ability to oxidize fatty acids in peroxisomes.

Knockdown of Pex16 in brown adipocytes does not increase mitochondrial ROS production. We next explored the possibility that mitochondrial dysfunction associated with impaired peroxisomal biogenesis could potentially be related to an altered mitochondrial redox state. Intracellular redox state is thought to influence mitochondrial dynamics (38). Moreover, oxidative stress has been reported to cause degradation of mitochondrial DNA (39). To determine if loss of peroxisomes affects mitochondrial redox state, we used a lentivirus-encoded redox-sensitive green fluorescent protein possessing a mitochondrial localization sequence (Mito-roGFP) to assess changes in mitochondrial ROS levels in BAT SVF cells treated with scrambled or Pex16 shRNA. This ratiometric sensor has certain surface-exposed residues mutated to cysteine, permitting dithiol formation, and it exhibits two excitation maxima, one at 400 nm (reflective of oxidative state) and another at the normal 484 nm (reflective of reductive state) (40). The ratio of fluorescence measured following differential excitation represents the mitochondrial redox state. Interestingly, knockdown of Pex16 decreased GFP fluorescence following excitation at either 400 or 484 nm (Supplemental Figure 8A), presumably reflecting the decreased mitochondrial mass due to the loss of peroxisomes and the ratio of two fluorescence readouts was unchanged in Pex16 knockdown cells as compared control cells (Supplemental Figure 8B). These data suggest that mitochondrial dysfunction due to impaired peroxisomal biogenesis is likely not due to increased mitochondrial oxidative stress.

Presence of peroxisome-derived phospholipids in mitochondria. Another potential mechanism for the mitochondrial dysfunction and impaired thermogenesis in the peroxisome deficient mice could be altered mitochondrial membrane phospholipid composition, leading to disruption of mitochondrial dynamics. To investigate this possibility, we determined if peroxisome-derived

lipids are present in mitochondria and if inhibition of their synthesis phenocopies the effects of disrupting peroxisomal biogenesis on mitochondrial morphology and function (Figure 8). Peroxisomes are critical for synthesis of ether lipids, a special class of phospholipids in which the hydrocarbon chain at the *sn-1* position of the glycerol backbone is attached by an ether bond, as opposed to an ester bond in the more common diacyl phospholipids(41, 42). Plasmalogens, the most common form of ether lipids, have a *cis* double bond adjacent to the ether bond. The initial steps of ether lipid synthesis take place in peroxisomes (Figure 8A). Notably, Pex16 knockout resulted in degradation of the plasmalogen synthetic enzymes AGPS and GNPAT in BAT and iWAT (Figure 8, B and C). Targeted lipidomics analysis of mitochondria isolated from BAT of wild-type mice indicated that plasmalogens are present at levels close to cardiolipins (CL) (Figure 8D), which are an important component of mitochondrial membranes (43). Since isolated mitochondria are known to be contaminated with other organelles, especially peroxisomes (44), we performed immunoblot analysis of mitochondrial and peroxisomal markers to assess the purity. Our results suggest that the mitochondrial fraction was enriched in known mitochondrial proteins COX IV and Tomm20, but had only small amounts of the peroxisomal proteins PMP70 and catalase (Supplemental Figure 9A). Moreover, our lipidomics analysis suggests that CL account for ~10% of the total phospholipids in BAT mitochondria, which is within the range of previously reported levels of 10-15% in the mitochondria of various cell types (43), suggesting that our isolated mitochondria are relatively pure.

Knockout of Pex16 reduced the levels of ethanolamine plasmalogens without affecting the total abundance of diacyl phosphatidylethanolamine (PE) (Figures 8, E and F) or CL (Supplemental Figure 9B). Ether-linked phosphatidylcholines (PC), including choline plasmalogens were

present in very low abundance in mitochondria and certain species of diacyl PC were increased with Pex16 knockout (Supplemental Figure 9C).

Inhibition of plasmalogen synthesis affects mitochondrial dynamics and function in adipocytes. We next determined if inhibition of plasmalogen synthesis affects mitochondrial morphology and function in cultured adipocytes. We previously identified the enzyme that catalyzes the terminal peroxisomal step in ether lipid synthesis and named the protein PexRAP (45). Since PexRAP also appears to have other functions related to regulation of gene expression and its inactivation results in only partial reduction in plasmalogens (46), we knocked down the expression of GNPAT, the enzyme responsible for the first step in plasmalogen production, to determine the effects on mitochondria. As observed with Pex16 knockdown, GNPAT knockdown during the late stage of differentiation in BAT SVF cells did not affect adipogenic gene expression or lipid droplet formation (Supplemental Figure 5, C and D). Interestingly, GNPAT knockdown markedly altered the mitochondrial morphology and decreased mtDNA (Figures 8, G and H), mimicking the effect of Pex16 knockdown (Figure 5). Moreover, basal and NE-stimulated rates of oxygen consumption were significantly decreased with GNPAT knockdown (Figure 8I), similarly to Pex16 knockdown (Figure 5E).

Dietary supplementation of plasmalogen precursors rescues thermogenesis in Pex16-AKO mice. Finally, we explored the possibility that restoration of plasmalogen levels could relieve mitochondrial defects and impaired thermogenesis in *Pex16-AKO* mice (Figure 9). To this end, we treated control and *Pex16-AKO* mice with a chow diet containing alkylglycerols (16:0-AG and 18:0-AG), ether lipid precursors that enter the synthetic pathway downstream of the

peroxisomal steps and are known to be incorporated into plasmalogens (41). Treatment of mice with this diet increased the levels of several species of ethanolamine plasmalogens in the mitochondria from BAT in *Pex16-AKO* mice (Figure 9A) and restored the total plasmalogen content in mitochondria to the control levels (Supplemental Figure 10A). TEM analysis in BAT from cold-treated mice indicates that AG treatment increased the circularity and abundance of mitochondria in *Pex16-AKO* mice (Figure 9, B-D), suggesting that restoration of plasmalogens rescues cold-induced division of mitochondria. Consistent with this notion, the AG-diet increased BAT mitochondrial DNA copy number in *Pex16-AKO* mice (Figure 9E), without affecting the expression of genes involved in mitochondrial biogenesis or dynamics (Supplemental Figure 10B). Indirect calorimetry showed that AG increased NE-stimulated oxygen consumption in control and Pex16-AKO mice (Figure 9F). Interestingly, this effect on oxygen consumption was not seen in animals housed at thermoneutrality (Supplemental Figure 10C), suggesting that plasmalogens promote energy expenditure by activating thermogenesis. In support of this possibility, the AG treatment rescued cold intolerance in *Pex16-AKO* mice (Figure 9G). The protective effects of AG required several weeks of treatment, whereas a short-term (1-week) treatment did not mitigate cold intolerance in *Pex16-AKO* mice (Supplemental Figure 10D). Although dietary AG is absorbed intact, the vinyl ether bond can be oxidized in the intestinal mucosal cells (41). As such, whereas plasma lipids change rapidly within a few days of dietary manipulation, changes in erythrocytes and other tissues requires several weeks of treatment (41, 47).

To understand systemic effects of AG, we determined its role in fatty acid and pyruvate oxidation in BAT, skeletal muscle and liver in *Pex16-AKO* and control mice. There were no

genotype-specific effects on palmitate or pyruvate oxidation in muscle and liver (Supplemental Figure 11, A-D). However, the AG treatment significantly decreased palmitate oxidation and resulted in a trend toward increased pyruvate oxidation in liver (Supplemental Figure 11, C and **D**). In BAT, Pex16 knockout impaired palmitate oxidation, but AG treatment did not improve this effect (Figure 9H). Interestingly, Pex16 inactivation also resulted in a trend toward impaired pyruvate oxidation, which was restored by AG in BAT (Figure 9I). The defect in glucose metabolism in *Pex16-AKO* mice is likely at the level of mitochondria in adipose tissue, since knockdown of Pex16 in cultured brown adipocytes did not block insulin-stimulated translocation of the Glut4 glucose transporter (Supplemental Figure 11E).

Together, these results support our notion that AG rescues thermogenesis in *Pex16-AKO* mice by relieving the defect in cold-induced mitochondrial division in adipose tissue. However, we cannot rule out the possibility that metabolism of AG by other tissues could potentially also contribute to its beneficial effects, since it increased VO_2 in both control and *Pex16-AKO* mice.

Discussion

Our studies suggest that peroxisomal biogenesis increases in adipose tissue in response to cold exposure, in a manner dependent on the thermogenic transcription factor PRDM16, suggesting that the transcriptional regulation of thermogenesis and de novo peroxisome formation is coordinated. Using mice with adipose-specific knockout of *Pex16*, we show that disruption of peroxisomal biogenesis impairs cold-induced adipose tissue thermogenesis without affecting thermogenic gene expression. The loss of peroxisomes also impaired diet-induced thermogenesis, resulting in late-onset obesity, similar to adipose-specific knockout of *Prdm16* in

mice (17), suggesting that PRDM16-mediated regulation of adiposity might be related to its control of peroxisomal biogenesis. Together, our results indicate that peroxisomes are critical for adipose tissue thermogenesis and the mice with adipose-specific peroxisome-deficiency have increased adiposity due to their inability to mount the diet-induced, norepinephrine-recruited thermogenic response.

Recent studies suggest that mitochondria are involved in de novo peroxisome formation (3). By pursuing the molecular mechanism through which peroxisomes regulate adipose tissue thermogenesis, our work suggests that peroxisomes are reciprocally involved in mitochondrial division. As highly dynamic organelles, mitochondria alter their abundance and morphology through fission and fusion processes, depending on metabolic context (26). Fragmented mitochondria are observed during nutrient excess (48). In contrast, elongated mitochondria are associated with conditions that require increased metabolic efficiency, such as starvation (49, 50). Mitochondrial elongation is also linked to decreased uncoupled respiration (28). Accordingly, previous studies show that β-adrenergic receptor activation-induced mitochondrial fission serves as a critical physiological regulator of energy expenditure and thermogenic function of brown adipocytes (23). Although the precise molecular mechanism is unclear, fragmented mitochondria are thought to exhibit increased uncoupled respiration by directing fatty acid oxidation toward heat production and energy expenditure, instead of ATP synthesis. Our studies suggest that the loss of peroxisomes blocks cold-induced mitochondrial fission in adipose tissue, resulting in elongated mitochondria, and impaired thermogenesis.

Unlike pan-adipose Pex16 inactivation, BAT-specific knockout of the peroxisomal biogenesis factor was not sufficient to fully impair thermogenesis, suggesting that beige fat plays a physiologically significant role in peroxisome-dependent regulation of thermogenesis. Like brown adipocytes, beige adipocytes are enriched in mitochondria. Increasing evidence supports the importance of beige adipocyte mitochondria in UCP1-dependent and –independent mechanisms of thermogenesis and regulation of adiposity and metabolism (32, 51, 52). Our results indicate that peroxisomes in both brown and beige fat may be involved in regulating mitochondrial dynamics and function to impact thermogenesis. However, a lack of Cre line that specifically targets WAT makes it difficult to experimentally distinguish the thermogenic contribution of beige fat from that of BAT and to assess other possible functions of Pex16 in WAT that could potentially impact adiposity and metabolism through mechanisms other than thermogenic regulation.

One potential explanation for the formation of elongated mitochondria due to Pex16 inactivation could be that peroxisome deficiency promotes mitochondrial fusion instead of impairing fission. However, the decreased mtDNA copy number argues against increased fusion being a primary effect. Regulation of mtDNA copy number is considered a primary role of mitochondrial dynamics (53). Consistent with the notion that peroxisome-deficiency results in impaired mitochondrial fission, our results suggest Pex16 inactivation in adipocytes causes mitochondria to elongate and form tubular network structures, as well as causing mtDNA loss and impaired mitochondrial function, phenocopying the previously reported effects of directly inhibiting mitochondrial fission through Drp1 inactivation (27-29).

Mitochondrial dysfunction in the context of peroxisome deficiency has been well documented for hepatocytes (54). Although the underlying molecular mechanism remains unknown, lack of peroxisomes in hepatocytes results in severe mitochondrial abnormalities, including destruction of the inner mitochondrial membrane, distortion of cristae structure, decreased membrane potential, and increased ROS production. Notably, these abnormalities appear to be selective for hepatocytes (55) and are all distinct from the mitochondrial changes resulting from the inhibition of peroxisomal biogenesis in adipocytes reported here. Unlike hepatocytes, which normally have numerous large nucleoid (crystalloid core)-containing peroxisomes (~0.7 μm diameter), other cell types, including adipocytes have fewer and smaller peroxisomes lacking nucleoid, referred to as microperoxisomes (~0.1 μm diameter) in older literature (56). In contrast to the effects of peroxisome deficiency in hepatocytes, our results suggest the mitochondria in the peroxisome-deficient adipocytes are visibly normal with intact cristae and unaffected membrane potential and without increased ROS production. Instead, our data strongly suggest that the primary defect in adipocytes is impaired mitochondrial division, resulting in mtDNA loss, decreased expression of mitochondrially-encoded components of the electron transport chain, and reduced rate of coupled and uncoupled respiration.

These phenotypes do not appear to be related to a loss of ability to oxidize VLCFAs or through an altered redox state in adipocytes in the absence of peroxisomes. Instead, peroxisomal plasmalogen synthesis appears to be involved in the mechanism. Due to the presence of a vinyl ether bond at the *sn-1* position of their glycerol backbone, plasmalogens tend to form non-lamellar lipid structures, such as inverted hexagonal configurations, suggesting that they might be involved in membrane dynamics (57, 58). Our results indicate that plasmalogens are present

in adipocyte mitochondria and disruption of their synthesis impairs mitochondrial fission, perhaps by altering biophysical properties of the outer mitochondrial membrane and blocking Drp1-mediated membrane constriction.

Collectively, our data suggest that peroxisomes regulate adipose tissue thermogenesis by directing plasmalogens to mitochondria to mediate mitochondrial fission. Manipulating plasmalogen production through dietary or pharmacological means could improve the thermogenic function of brown and beige fat, perhaps leading to a novel treatment option for obesity.

Methods

Mouse models. *PRDM16*$^{Lox/Lox}$ mice were obtained from the Jackson Laboratory (stock no. 024992) and have been previously described (17). Pex16 conditional-potential mice were obtained from the EUCOMM repository. To generate mice with conditional alleles of *Pex16*, the lacZ/neo selection cassette was removed by crossing the mice with transgenic mice expressing Flp recombinase under the control of the actin promoter (The Jackson Laboratory). The Flp transgene was selected against in subsequent crosses. *Acox1*$^{Lox/Lox}$ mice were generated using the CRISPR/Cas9 system. CRISPR-mediated mutagenesis was done by the Genome Engineering and IPSC Center (GEiC) at Washington University. The CRISPR nucleases were validated to ensure that they cut the desired endogenous chromosomal target sites. All successful mutants were verified through deep sequencing. To generate mice with adipose-specific knockout of *Prdm16*, *Pex16* or *Acox1*, floxed mice for each line were crossed with *adiponectin-Cre* transgenic mice (18). To generate BAT-specific *Pex16* knockout mice, *Pex16*$^{Lox/Lox}$ were crossed

with *Ucp1-Cre* mice (59). For each line, respective floxed mice without Cre were used as control. Mice were housed at room temperature (22^{o}C) and fed PicoLab Rodent Diet 20 control chow or Harlan Teklad TD 88137 high-fat diet (42% calories from fat), as indicated. For thermoneutrality experiments, the mice were housed at 30^{o}C. The alkylglycerol diet was generated by incorporating 1g/kg each of 1-O-hexadecyl-rac-glycerol (Chem-Impex International, Wood Dale, IL) and 1-O-octadecyl-rac-glycerol (Bachem, Torrance, CA) to PicoLab Rodent Diet 20. For cold tolerance studies, mice were individually housed at 4^{o}C and rectal temperature was measured using an Extech thermocouple thermometer. For other analysis related to cold exposure, mice were housed together at 4^{o}C for 48 hours, unless otherwise noted.

***Cell lines*.** Human embryonic kidney 293T (HEK293T) cells and COS-7 cells were maintained in Dulbecco's modified Eagle's medium (DMEM) supplemented with 10% FBS. Stromal vascular fractions from mouse iWAT and BAT were isolated, immortalized and differentiated into adipocytes as previously reported (46). Briefly, confluent BAT SVF cells were treated with DMEM/F12 supplemented with 0.5 μM isobutylmethylxanthine, 5μM dexamethasone, 125μM indomethacin, 1 μM rosiglitazone, 1 nM T3, and 0.02 μM insulin. After two days, the cells were switched to medium supplemented only with 1 nM T3 and 0.02 μM insulin (maintenance medium), which was replaced every 2 days. iWAT SVF cells were differentiated into adipocytes as previously described (60).

***Antibodies*.** Rabbit polyclonal antibodies against actin (1:3000; catalog no. A2066) and PMP70-Atto-488 (1:100; catalog no. P0090) as well as mouse monoclonal antibodies against FLAG (1:1000; catalog no. F1804) and PMP70 (1:2000; catalog no. SAB4200181) and mouse

polyclonal antibody against Pex14 (1:1000; catalog no. SAB1409439) were from Sigma (St. Louis, MO). Rabbit polyclonal antibodies against Pex16 (1:1000; catalog no. 14816-1-AP), Acox1 (1:1000; catalog no. 10957-1-AP) and GNPAT (1:1000; catalog no. 14931-1-AP) were from Proteintech (Rosemont, IL). Rabbit polyclonal anti-FAS antibody (1:5000; catalog no. ab22759) was purchased from Abcam (Cambridge, MA). Anti-UCP1 rabbit antibody (1:1000; catalog no. UCP11-A) was purchased from Alpha Diagnostics (San Antonio, TX). Mouse monoclonal antibodies against COX IV (1:1000; catalog no. 11967S) and Drp1(1:1000; catalog no. 14647S) and a rabbit polyclonal antibody against Tomm22 (1:1000; catalog no. 42406S) were from Cell Signaling Technology (Danvers, MA). Anti-β-tubulin rabbit polyclonal (1:1000; SC-9104) and anti-AGPS mouse monoclonal (1:1000; catalog no. SC-374201) antibodies were from Santa Cruz Biotechnology (Santa Cruz, CA). Light chain-specific HRP-conjugated secondary antibodies (1:2500; catalog nos. 211-032-171 and 115-035-174) were from Jackson ImmunoResearch (West Grove, PA).

***Plasmid Constructs*.** To construct the Pex16-eGFP reporter construct, a -2 kb Pex16 promoter was amplified by PCR using liver genomic DNA from a wild-type C57 mouse and cloned into pEGFP-N1 plasmid in the place of the CMV promoter. To generate the Pex16-Luciferase reporter plasmid, the gene encoding the firefly luciferase was amplified by PCR using the PPRE X3-TK-luc plasmid (Addgene) as template. The luciferase gene was then cloned into the Pex16-eGFP plasmid in the place of eGFP using the restriction enzymes AgeI and NotI. To create the lentiviral Mito-roGFP construct, roGFP containing a mitochondrial localization sequence was amplified by PCR using a previously generated adenoviral Matrix-roGFP2 (Addgene plasmid #49437) construct as template (40). The resulting amplicon was cloned into pLJM1-EGFP

plasmid (Addgene plasmid #19319) in place of EGFP using restriction sites AgeI and EcoRI. The lentiviral plasmid pLenti-Myc-Glut4-mCherry was obtained from Addgene (plasmid #64049) and has been previously described (61).

ChIP-qPCR Assays. ChIP studies were conducted using the SimpleChIP Enzymatic Chromatin IP Kit (Cell Signaling Technology) according to manufacturer's instruction. Briefly, BAT SVF cells stably expressing FLAG-tagged PRM16 were fixed with 1% formaldehyde for 15 min. Nuclei were harvested and chromatin digested by micrococcal nuclease before being lysed on ice by 3 sets of 10-second pulses from a Sonics VCX 500 probe sonicator at 30% amplitude. Chromatin was clarified by centrifugation before being incubated with FLAG M2 antibodies at 4^{o}C overnight. ChIP-Grade protein G agarose beads were incubated for 4 hours, spun, and washed. Crosslinks were reversed and DNA was purified by spin column. DNA was quantified by qPCR using PowerUp SYBR Green Master Mix (Thermo Fisher) in triplicate and data are shown as percentage of input. Primer sequences used in qPCR are provided in Supplemental Table 1.

Indirect Calorimetry. To measure basal oxygen consumption (VO_2), carbon dioxide production (VCO_2), and respiratory exchange ratio (RER) in HFD-fed animals, a Phenomaster (TSE Systems) metabolic cage system was used. Mice were acclimated to the system for 24 hr prior to taking measurements. To measure NE-stimulated VO_2 in mice, an Oxymax Eco System (Columbus Instruments) was used. The mice were acclimated to the system for 4 hrs. The rate of oxygen consumption was measured for 20 min prior to and 60 min after administering NE (1 mg/kg, i.p. injection).

Measurement of Oxygen Consumption Rate in Cultured Adipocytes. Oxygen consumption rate (OCR) in control and Pex16 knockdown BAT SVF cells was measured using XF24 Extracellular Flux Analyzer with a FluxPak (Seahorse Bioscience). The cells were seeded and grown to confluence on XF24 cell culture microplates before treatment with differentiation media, as previously described (46). At day two, the cells were treated with scrambled or Pex16 shRNA lentivirus in the maintenance media. After 72 hr treatment, the viral media were removed and replaced with fresh maintenance media. At day eight of differentiation, OCR was measured at 3 min intervals at baseline and after the addition of 2 µM norepinephrine, 3 µM oligomycin, 2 µM antimycin A and 1 µM rotenone.

High Resolution Respirometry. Mitochondrial respiration in BAT and iWAT from *Pex16-AKO* and control mice was measured using a modification of a previously reported method (62). After excision, adipose samples were immersed in cold BIOPS (10 mM EGTA, 50 mM MES, 0.5 mM DTT, 6.56 mM $MgCL_2$, 5.77 mM ATP, 20 mM imidazole and 15 mM phosphocreatine, pH 7.1) until tissue preparation. After all samples were collected, tissue was blotted dry, weighed and then minced in to approximately 2 mg pieces with scissors. Minced samples were placed in the pre-warmed Oroboros chambers with mitochondrial respiration solution MiR05 (0.5 mM EGTA, 3 mM $MgCl_2$, 60 mM K-lactobionate, 20 mM taurin, 10 mM KH_2PO_4, 20 mM HEPES, 110 mM sucrose and 1 g/L BSA, pH 7.1). Digitonin (2 µM) was added to each chamber to permeabilize the samples. Oxygen was added to each chamber to ensure oxygen availability within the tissue pieces. Oxygen levels were maintained above 250 pmol during the assay. To measure O_2 flux, the following substrates were added sequentially: octanoyl carnitine (1.5 mM),

pyruvate (5 mM), glutamate (10 mM) and malate (2 mM), ADP (20 mM) and succinate (20 mM), followed by 3 pulses of 0.5 µM FCCP. A period of stabilization followed the addition of each substrate and the oxygen flux per mass was recorded using the DatLab 6.1 Software (OROBOROS Instruments, Innsbruck, Austria).

***Transmission Electron Microscopy*.** For TEM analysis of BAT, control and *Pex16-AKO* mice were sacrificed and perfused with warm Ringer's solution for 2 minutes at 37°C, followed by 2% para-formaldehyde plus 2.5% glutaraldehyde, in 0.09M cacodylate buffer, pH 7 .2, containing 5% sucrose and 0.025% $CaCl_2$ at 37˚C for 5 minutes. Peroxisomes were visualized by staining with 3,3'-diaminobenizidine (DAB) as previously described (63) and images were acquired using a JEOL JEM-1400Plus Transmission Electron Microscope.

***Mitochondrial DNA Copy Number*.** Total genomic DNA was isolated from brown fat tissue or BAT SVF cells using DNeasy Blood & Tissue Kit (Qiagen). Mitochondrial DNA copy number normalized to nuclear DNA was measured by qPCR using 50 ng of total genomic DNA and PowerUp SYBR Green reagent. Primer sequences for mitochondrial and nuclear DNA are as follows: mitoDNA-Fwd: TTA-AGA-CAC-CTT-GCC-TAG-CCA-CAC; mitoDNA-Rev: CGG-TGG-CTG-GCA-CGA-AAT-T; NucDNA-Fwd: ATG-ACG-ATA-TCG-CTG-CGC-TG; NucDNA-Rev: TCA-CTT-ACC-TGG-TGC-CTA-GGG-C.

***Mitochondrial Morphology Assay*.** BAT SVF cells stably expressing Mito-roGFP were seeded in 24-well plates with high performance #1.5 cover glass bottoms (Cellvis #P24-1.5H-N), grown to confluence and then treated with brown adipocyte differentiation cocktail as previously

described (46). On 4 days following the initiation of differentiation, the cells were infected with scrambled, Pex16, or GNPAT shRNA lentivirus in the differentiation medium. After 24 hrs, the viral medium was removed and fresh differentiation medium was added. On day 9 of differentiation, the medium was removed and the cells were washed with pre-warmed PBS before addition of phenol red free-DMEM containing a 10% solution of BackDrop Background Suppressor (Invitrogen) and the cells were imaged using a Nikon A1Rsi Confocal Microscope. Mitochondrial morphology was quantified by visual inspection and cells were divided into three groups exhibiting fragmented, fused or intermediate (partially fragmented) mitochondria, as previously described (23).

Oxidation Assays. BAT, muscle or liver from control and *Pex16 AKO* mice was homogenized in a buffer containing 250 mM sucrose, 1 mM EDTA, 10 mM Tris-HCl and 2 mM ATP in a glass homogenization tube with a motor-teflon pestle at 4^{o}C. Following homogenization, tissue homogenates were transferred to 1.5 microcentrifuge tubes and centrifuged at 1000 g for 10 min at 4^{o}C. Supernatant was obtained and protein concentration was measured. 40 µL of homogenate was added to a 48 well plate with adjacent wells connected by a fabricated groove. 200 µl 1 M NaOH was added to wells adjacent to sample wells to trap CO_2 generated by the oxidation reaction. A 160 µL aliquot of reaction mixture was then added to sample wells and then sealed with parafilm covered by a rubber gasket. Final concentration of reagents in the mixture were 100 mM sucrose, 10 mM Tris-HCl, 5 mM KH_2PO_4, 100 mM KCl, 1mM $MgCl_2$, 1 mM L-carnitine, 0.1 mM malate, 2 mM ATP, 0.05 mM coenzyme A, 1 mM DTT, and either 0.1 mM palmitate ([1-^{14}C] palmitate 0.5 µCi/ml) in 0.5% BSA, 0.1 mM sodium pyruvate ([2-^{14}C] sodium pyruvate 0.5 µCi/ml) in 0.5% BSA or 0.025 mM lignoceric acid ([1-^{14}C] lignoceric acid 0.5

μCi/ml) in 25 mg/ml α-cyclodextrin. After 60 min (palmitate and pyruvate) or 4 hours (lignoceric acid) incubation at 37°C, 100 μl of 70% perchloric acid was injected to sample wells to stop the reaction. CO_2 generated during incubations was trapped in adjoining wells containing NaOH. The plates were then placed on a shaker for an additional 1 hr at RT, and then 150 μL of NaOH was transferred to scintillation fluid and counted.

The effect of Acox1 knockout on VLCFA oxidation was determined by measuring catabolism of stable-isotope labelled docosanoic acid (D_3-C22:0) to D_3-C16:0 via mass spectrometric analysis, as previously described (64). Briefly, iWAT SVF cells were harvested from $Acox1^{Lox/Lox}$ mice and treated with pBABE-Cre or empty vector. Following selection with 2 μg/ml puromycin for three days, the normal medium was switched to lipid-free FBS-containing medium supplemented with 30 μM (22, 22, 22) D_3-C22:0. The cells were harvested using a buffer containing 20 μM LiCl to perform lipid extraction, followed by mass spectrometric analysis.

Statistics. Results containing error bars are expressed as mean±SEM. Comparisons between two groups were performed using two-tailed Student's t test. To assess statistical significance in the survival curves, Mantel-Cox (log-rank) test was used. ANOVA was used for more than two groups. Statistical significance is represented as follows: *P<0.05, **P<0.01, ***P<0.001, n.s., not significant.

Study Approval. All animal experiments were performed in accordance with procedures approved by the Institutional Animal Care and Use Committee at Washington University School of Medicine.

Author contributions

H.P. and A.H. conceived hypotheses, designed and conducted experiments and performed data analyses. J.M.J., J.M.D. and T.A.P. conducted experiments and performed data analysis. M.T., Y.C. and X.Z. performed experiments. F.-F.H. performed mass spectrometry analyses, assigned structures of lipid molecules, and interpreted data. K.F. and B.R. designed experiments. I.J.L. conceived the study, designed experiments, performed data analysis and wrote the paper.

Acknowledgments

This work was supported by NIH grants R00-DK094874 (I.J.L.), R01-DK115867 (I.J.L.), R01-DK107397 (K.F.), R03-DK109888 (K.F.), and R01-HL125838 (B.R.). I.J.L. was also supported by funds from the Diabetes Research Center (P30-DK020579) and by a pilot & feasibility grant from the Nutrition Obesity Research Center (P30-DK56341) at Washington University. H.P. was supported by Diabetes Research Postdoctoral Training Program fellowship (T32-DK007120). A.H. was supported in part by funds from the China Scholarship Council (201506140012). Lipid mass spectrometry work was supported by P41-GM103422. The authors thank Dr. Clay Semenkovich for critical reading of the manuscript and helpful discussions and Dr. Jeffrey Millman for advice on oxygen consumption assays using the Seahorse XF24 Extracellular Flux Analyzer.

Address correspondence to: Irfan J. Lodhi, Washington University School of Medicine, Division of Endocrinology, Metabolism and Lipid Research, 660 S. Euclid Avenue, Saint Louis, MO 63110, USA; Phone: 314.747.6766; Email: ilodhi@wustl.edu

Conflict of interest: The authors have declared that no conflict of interest exists.

References

1. Ahlabo I, and Barnard T. Observations on peroxisomes in brown adipose tissue of the rat. *The journal of histochemistry and cytochemistry : official journal of the Histochemistry Society.* 1971;19(11):670-5.
2. Lodhi IJ, and Semenkovich CF. Peroxisomes: a nexus for lipid metabolism and cellular signaling. *Cell Metab.* 2014;19(3):380-92.
3. Sugiura A, Mattie S, Prudent J, and McBride HM. Newly born peroxisomes are a hybrid of mitochondrial and ER-derived pre-peroxisomes. *Nature.* 2017;542(7640):251-4.
4. Agrawal G, and Subramani S. De novo peroxisome biogenesis: Evolving concepts and conundrums. *Biochim Biophys Acta.* 2016;1863(5):892-901.
5. Braverman NE, Raymond GV, Rizzo WB, Moser AB, Wilkinson ME, Stone EM, et al. Peroxisome biogenesis disorders in the Zellweger spectrum: An overview of current diagnosis, clinical manifestations, and treatment guidelines. *Molecular genetics and metabolism.* 2016;117(3):313-21.
6. Jones JM, Morrell JC, and Gould SJ. PEX19 is a predominantly cytosolic chaperone and import receptor for class 1 peroxisomal membrane proteins. *J Cell Biol.* 2004;164(1):57-67.
7. Gould SG, Keller GA, and Subramani S. Identification of a peroxisomal targeting signal at the carboxy terminus of firefly luciferase. *J Cell Biol.* 1987;105(6 Pt 2):2923-31.
8. Swinkels BW, Gould SJ, Bodnar AG, Rachubinski RA, and Subramani S. A novel, cleavable peroxisomal targeting signal at the amino-terminus of the rat 3-ketoacyl-CoA thiolase. *The EMBO journal.* 1991;10(11):3255-62.
9. Dodt G, and Gould SJ. Multiple PEX genes are required for proper subcellular distribution and stability of Pex5p, the PTS1 receptor: evidence that PTS1 protein import is mediated by a cycling receptor. *J Cell Biol.* 1996;135(6 Pt 2):1763-74.
10. Braverman N, Steel G, Obie C, Moser A, Moser H, Gould SJ, et al. Human PEX7 encodes the peroxisomal PTS2 receptor and is responsible for rhizomelic chondrodysplasia punctata. *Nature genetics.* 1997;15(4):369-76.
11. Bagattin A, Hugendubler L, and Mueller E. Transcriptional coactivator PGC-1alpha promotes peroxisomal remodeling and biogenesis. *Proc Natl Acad Sci U S A.* 2010;107(47):20376-81.
12. Guardiola-Diaz HM, Rehnmark S, Usuda N, Albrektsen T, Feltkamp D, Gustafsson JA, et al. Rat peroxisome proliferator-activated receptors and brown adipose tissue function during cold acclimatization. *J Biol Chem.* 1999;274(33):23368-77.
13. Nedergaard J, Alexson S, and Cannon B. Cold adaptation in the rat: increased brown fat peroxisomal beta-oxidation relative to maximal mitochondrial oxidative capacity. *The American journal of physiology.* 1980;239(5):C208-16.
14. Martens K, Bottelbergs A, Peeters A, Jacobs F, Espeel M, Carmeliet P, et al. Peroxisome deficient aP2-Pex5 knockout mice display impaired white adipocyte and muscle function

concomitant with reduced adrenergic tone. *Molecular genetics and metabolism.* 2012;107(4):735-47.
15. Wang W, and Seale P. Control of brown and beige fat development. *Nat Rev Mol Cell Biol.* 2016;17(11):691-702.
16. Ohno H, Shinoda K, Spiegelman BM, and Kajimura S. PPARgamma agonists induce a white-to-brown fat conversion through stabilization of PRDM16 protein. *Cell Metab.* 2012;15(3):395-404.
17. Cohen P, Levy JD, Zhang Y, Frontini A, Kolodin DP, Svensson KJ, et al. Ablation of PRDM16 and beige adipose causes metabolic dysfunction and a subcutaneous to visceral fat switch. *Cell.* 2014;156(1-2):304-16.
18. Eguchi J, Wang X, Yu S, Kershaw EE, Chiu PC, Dushay J, et al. Transcriptional control of adipose lipid handling by IRF4. *Cell Metab.* 2011;13(3):249-59.
19. Harms MJ, Ishibashi J, Wang W, Lim HW, Goyama S, Sato T, et al. Prdm16 is required for the maintenance of brown adipocyte identity and function in adult mice. *Cell Metab.* 2014;19(4):593-604.
20. Aranovich A, Hua R, Rutenberg AD, and Kim PK. PEX16 contributes to peroxisome maintenance by constantly trafficking PEX3 via the ER. *J Cell Sci.* 2014;127(Pt 17):3675-86.
21. Lodhi IJ, and Semenkovich CF. Why we should put clothes on mice. *Cell Metab.* 2009;9(2):111-2.
22. Butler AA, and Kozak LP. A recurring problem with the analysis of energy expenditure in genetic models expressing lean and obese phenotypes. *Diabetes.* 2010;59(2):323-9.
23. Wikstrom JD, Mahdaviani K, Liesa M, Sereda SB, Si Y, Las G, et al. Hormone-induced mitochondrial fission is utilized by brown adipocytes as an amplification pathway for energy expenditure. *The EMBO journal.* 2014;33(5):418-36.
24. Mishra P, and Chan DC. Metabolic regulation of mitochondrial dynamics. *J Cell Biol.* 2016;212(4):379-87.
25. Hofer DC, Pessentheiner AR, Pelzmann HJ, Schlager S, Madreiter-Sokolowski CT, Kolb D, et al. Critical role of the peroxisomal protein PEX16 in white adipocyte development and lipid homeostasis. *Biochim Biophys Acta Mol Cell Biol Lipids.* 2017;1862(3):358-68.
26. Liesa M, and Shirihai OS. Mitochondrial dynamics in the regulation of nutrient utilization and energy expenditure. *Cell Metab.* 2013;17(4):491-506.
27. Ishihara N, Nomura M, Jofuku A, Kato H, Suzuki SO, Masuda K, et al. Mitochondrial fission factor Drp1 is essential for embryonic development and synapse formation in mice. *Nature cell biology.* 2009;11(8):958-66.
28. Parone PA, Da Cruz S, Tondera D, Mattenberger Y, James DI, Maechler P, et al. Preventing mitochondrial fission impairs mitochondrial function and leads to loss of mitochondrial DNA. *PLoS One.* 2008;3(9):e3257.
29. Wakabayashi J, Zhang Z, Wakabayashi N, Tamura Y, Fukaya M, Kensler TW, et al. The dynamin-related GTPase Drp1 is required for embryonic and brain development in mice. *J Cell Biol.* 2009;186(6):805-16.
30. Cassidy-Stone A, Chipuk JE, Ingerman E, Song C, Yoo C, Kuwana T, et al. Chemical inhibition of the mitochondrial division dynamin reveals its role in Bax/Bak-dependent mitochondrial outer membrane permeabilization. *Dev Cell.* 2008;14(2):193-204.

31. Ikeda K, Kang Q, Yoneshiro T, Camporez JP, Maki H, Homma M, et al. UCP1-independent signaling involving SERCA2b-mediated calcium cycling regulates beige fat thermogenesis and systemic glucose homeostasis. *Nat Med.* 2017;23(12):1454-65.
32. Kazak L, Chouchani ET, Jedrychowski MP, Erickson BK, Shinoda K, Cohen P, et al. A creatine-driven substrate cycle enhances energy expenditure and thermogenesis in beige fat. *Cell.* 2015;163(3):643-55.
33. Lee J, Ellis JM, and Wolfgang MJ. Adipose fatty acid oxidation is required for thermogenesis and potentiates oxidative stress-induced inflammation. *Cell Rep.* 2015;10(2):266-79.
34. Fan CY, Pan J, Usuda N, Yeldandi AV, Rao MS, and Reddy JK. Steatohepatitis, spontaneous peroxisome proliferation and liver tumors in mice lacking peroxisomal fatty acyl-CoA oxidase. Implications for peroxisome proliferator-activated receptor alpha natural ligand metabolism. *J Biol Chem.* 1998;273(25):15639-45.
35. Sassa T, and Kihara A. Metabolism of very long-chain Fatty acids: genes and pathophysiology. *Biomol Ther (Seoul).* 2014;22(2):83-92.
36. Fan CY, Pan J, Chu R, Lee D, Kluckman KD, Usuda N, et al. Hepatocellular and hepatic peroxisomal alterations in mice with a disrupted peroxisomal fatty acyl-coenzyme A oxidase gene. *J Biol Chem.* 1996;271(40):24698-710.
37. Ferdinandusse S, Denis S, van Roermund CWT, Preece MA, Koster J, Ebberink MS, et al. A novel case of ACOX2 deficiency leads to recognition of a third human peroxisomal acyl-CoA oxidase. *Biochim Biophys Acta Mol Basis Dis.* 2018;1864(3):952-8.
38. Shutt T, Geoffrion M, Milne R, and McBride HM. The intracellular redox state is a core determinant of mitochondrial fusion. *EMBO Rep.* 2012;13(10):909-15.
39. Shokolenko I, Venediktova N, Bochkareva A, Wilson GL, and Alexeyev MF. Oxidative stress induces degradation of mitochondrial DNA. *Nucleic Acids Res.* 2009;37(8):2539-48.
40. Waypa GB, Marks JD, Guzy R, Mungai PT, Schriewer J, Dokic D, et al. Hypoxia triggers subcellular compartmental redox signaling in vascular smooth muscle cells. *Circ Res.* 2010;106(3):526-35.
41. Braverman NE, and Moser AB. Functions of plasmalogen lipids in health and disease. *Biochim Biophys Acta.* 2012;1822(9):1442-52.
42. Dean JM, and Lodhi IJ. Structural and functional roles of ether lipids. *Protein Cell.* 2018;9(2):196-206.
43. Martensson CU, Doan KN, and Becker T. Effects of lipids on mitochondrial functions. *Biochim Biophys Acta Mol Cell Biol Lipids.* 2017;1862(1):102-13.
44. Benador IY, Veliova M, Mahdaviani K, Petcherski A, Wikstrom JD, Assali EA, et al. Mitochondria Bound to Lipid Droplets Have Unique Bioenergetics, Composition, and Dynamics that Support Lipid Droplet Expansion. *Cell Metab.* 2018;27(4):869-85 e6.
45. Lodhi IJ, Yin L, Jensen-Urstad AP, Funai K, Coleman T, Baird JH, et al. Inhibiting adipose tissue lipogenesis reprograms thermogenesis and PPARgamma activation to decrease diet-induced obesity. *Cell Metab.* 2012;16(2):189-201.
46. Lodhi IJ, Dean JM, He A, Park H, Tan M, Feng C, et al. PexRAP Inhibits PRDM16-Mediated Thermogenic Gene Expression. *Cell Rep.* 2017;20(12):2766-74.
47. Farquhar JW, and Ahrens EH, Jr. Effects of dietary fats on human erythrocyte fatty acid patterns. *J Clin Invest.* 1963;42:675-85.

48. Molina AJ, Wikstrom JD, Stiles L, Las G, Mohamed H, Elorza A, et al. Mitochondrial networking protects beta-cells from nutrient-induced apoptosis. *Diabetes.* 2009;58(10):2303-15.
49. Gomes LC, Di Benedetto G, and Scorrano L. During autophagy mitochondria elongate, are spared from degradation and sustain cell viability. *Nature cell biology.* 2011;13(5):589-98.
50. Rambold AS, Kostelecky B, Elia N, and Lippincott-Schwartz J. Tubular network formation protects mitochondria from autophagosomal degradation during nutrient starvation. *Proc Natl Acad Sci U S A.* 2011;108(25):10190-5.
51. Altshuler-Keylin S, Shinoda K, Hasegawa Y, Ikeda K, Hong H, Kang Q, et al. Beige Adipocyte Maintenance Is Regulated by Autophagy-Induced Mitochondrial Clearance. *Cell Metab.* 2016;24(3):402-19.
52. Shabalina IG, Petrovic N, de Jong JM, Kalinovich AV, Cannon B, and Nedergaard J. UCP1 in brite/beige adipose tissue mitochondria is functionally thermogenic. *Cell Rep.* 2013;5(5):1196-203.
53. Friedman JR, and Nunnari J. Mitochondrial form and function. *Nature.* 2014;505(7483):335-43.
54. Baes M, and Van Veldhoven PP. Hepatic dysfunction in peroxisomal disorders. *Biochim Biophys Acta.* 2016;1863(5):956-70.
55. Shinde AB, Baboota RK, Denis S, Loizides-Mangold U, Peeters A, Espeel M, et al. Mitochondrial disruption in peroxisome deficient cells is hepatocyte selective but is not mediated by common hepatic peroxisomal metabolites. *Mitochondrion.* 2018;39:51-9.
56. Novikoff AB, Novikoff PM, Rosen OM, and Rubin CS. Organelle relationships in cultured 3T3-L1 preadipocytes. *J Cell Biol.* 1980;87(1):180-96.
57. Koivuniemi A. The biophysical properties of plasmalogens originating from their unique molecular architecture. *FEBS Lett.* 2017;591(18):2700-13.
58. Lohner K. Is the high propensity of ethanolamine plasmalogens to form non-lamellar lipid structures manifested in the properties of biomembranes? *Chem Phys Lipids.* 1996;81(2):167-84.
59. Kong X, Banks A, Liu T, Kazak L, Rao RR, Cohen P, et al. IRF4 is a key thermogenic transcriptional partner of PGC-1alpha. *Cell.* 2014;158(1):69-83.
60. Fisher FM, Kleiner S, Douris N, Fox EC, Mepani RJ, Verdeguer F, et al. FGF21 regulates PGC-1alpha and browning of white adipose tissues in adaptive thermogenesis. *Genes Dev.* 2012;26(3):271-81.
61. Lim CY, Bi X, Wu D, Kim JB, Gunning PW, Hong W, et al. Tropomodulin3 is a novel Akt2 effector regulating insulin-stimulated GLUT4 exocytosis through cortical actin remodeling. *Nature communications.* 2015;6:5951.
62. Porter C, Herndon DN, Chondronikola M, Chao T, Annamalai P, Bhattarai N, et al. Human and Mouse Brown Adipose Tissue Mitochondria Have Comparable UCP1 Function. *Cell Metab.* 2016;24(2):246-55.
63. Fahimi HD. Cytochemical Detection of Peroxisomes in Light and Electron Microscopy with 3,3'-diaminobenzidine. *Methods Mol Biol.* 2017;1595:93-100.
64. van de Beek MC, Dijkstra IM, and Kemp S. Method for Measurement of Peroxisomal Very Long-Chain Fatty Acid Beta-Oxidation and De Novo C26:0 Synthesis Activity in Living Cells Using Stable-Isotope Labeled Docosanoic Acid. *Methods Mol Biol.* 2017;1595:45-54.

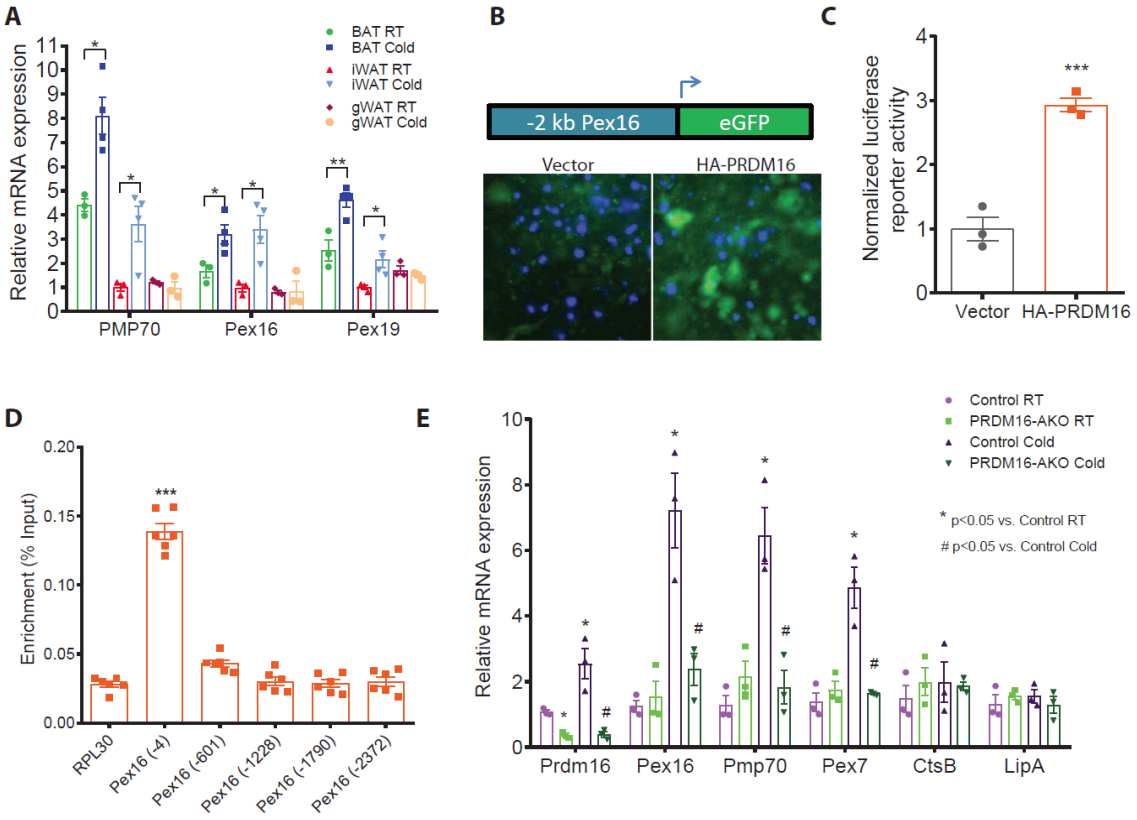

Figure 1. PRDM16 regulates cold-induced peroxisomal biogenesis in adipose tissue. (A) Gene expression analysis in BAT, iWAT and gWAT of wild-type mice kept at normal room temperature (22ºC) or subjected to cold (4ºC) exposure; n=3-4. (**B**) Fluorescence microscopy analysis of COS-7 cells transfected with a GFP reporter under the control of a -2 kb Pex16 promoter alone or together with HA-PRDM16. (**C**) Luciferase reporter assay in COS-7; n=3. (**D**) BAT SVF cells expressing retrovirally-encoded FLAG-PRDM16 were subjected to chromatin immunoprecipitation assay using an anti-FLAG antibody followed by qPCR using primers to amplify various regions of the Pex16 promoter; n=6. (**E**) Gene expression analysis in iWAT of control and adipose-specific PRDM16 knockout (*PRDM16-AKO*) mice; n=3. Data are expressed mean±SEM. and were analyzed by Student's t-test. *P<0.05; **P<0.01; ***P<0.001.

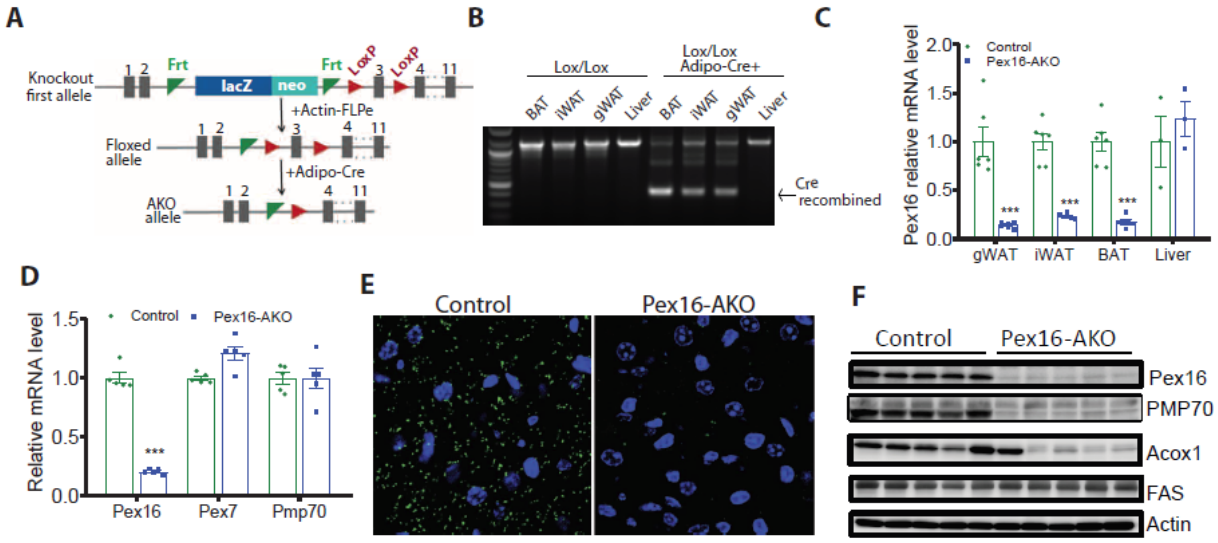

Figure 2. Generation of mice with adipose-specific knockout of Pex16. (**A**) Gene targeting strategy for Pex16 conditional knockout mice. (**B**) Analysis of Cre-mediated recombination by PCR. (**C**) Gene expression analysis; n=3-6. (**D**) Quantitative real-time PCR analysis demonstrating that Pex16 knockout does not affect gene expression of other peroxisomal genes in BAT; n=5. (**E**) Immunofluorescence analysis using anti-PMP70-Atto 488 antibody in BAT of control and *Pex16-AKO* mice. (**F**) Western blot analysis in iWAT. Data in panels C and D are expressed as mean±SEM and were analyzed by Student's t-test; ***P<0.001.

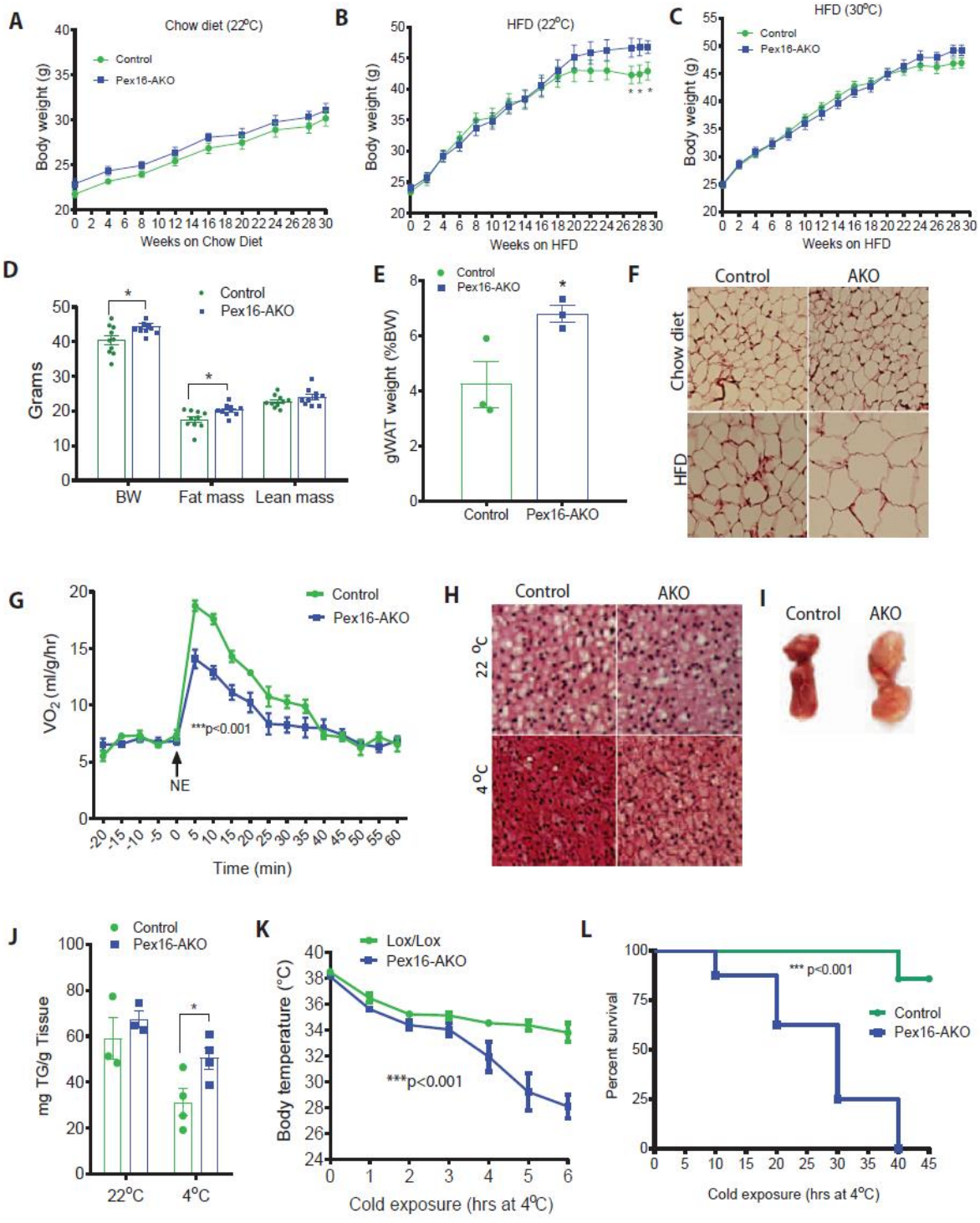

Figure 3. ***Pex16-AKO*** **mice have increased diet-induced obesity and impaired thermogenesis.** (**A**) Body weight of mice fed normal chow diet; n=7-9. (**B**) Body weight of mice fed a high fat diet and maintained at 22ºC; n=9-11. (**C**) Body weight of mice fed a high fat diet and maintained at 30ºC; n=8. (**D**) MRI analysis of body composition in room temperature-kept mice after 20 weeks of high fat feeding; n=10. (**E**) Weight of gWAT from HFD-fed mice; n=3. (**F**) H&E staining of

gWAT from chow and HFD fed control and *Pex16-AKO* mice. The images are representative of 3 mice per genotype. (**G**) Oxygen consumption rate (VO_2) before and after intraperitoneal norepinephrine injection; n=3-4. (**H**) H&E staining of BAT mice kept at room temperature or subjected to cold exposure. The images are representative of 3 mice per genotype. (**I**) Representative images (n=3) of BAT from cold-treated mice. (**J**) Quantification of triglycerides in BAT; n=3-4. (**K**) Rectal temperature of mice subjected to a 6 hr cold challenge; n=7-9. (**L**) Kaplan-Meier survival curves of mice individually-housed in InfraMot activity monitors stored at 4^{o}C; n=7-8. Data are expressed as mean±SEM. Student's t-test was used for analysis of the data in panels B, D, E and J. Two-way ANOVA with Bonferroni post test was used for analysis of the data in panels G and K. To assess statistical significance in panel L, Mantel-Cox (log-rank) test was used. *P<0.05; **P<0.01; ***P<0.001.

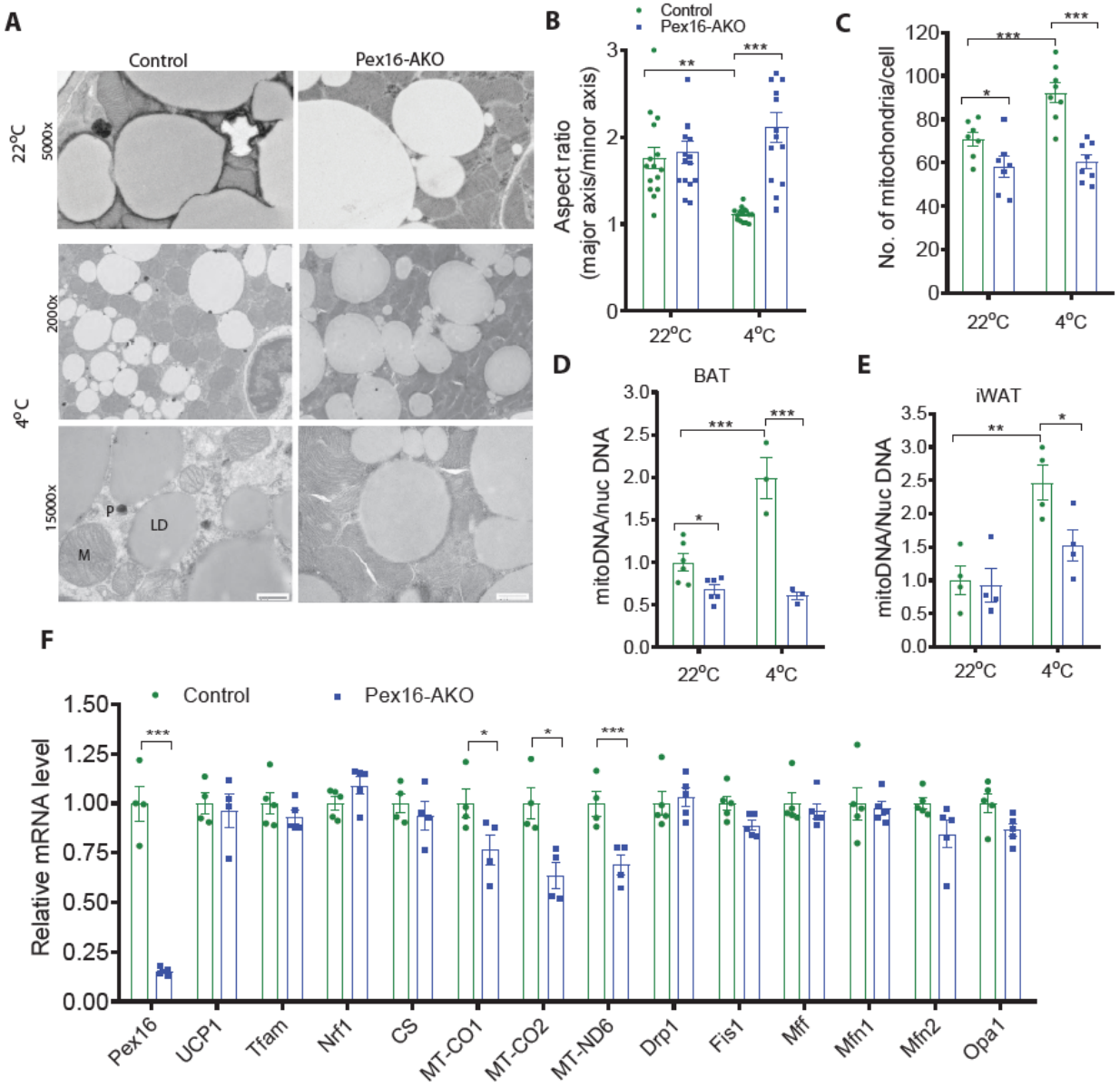

Figure 4. Pex16 inactivation impairs mitochondrial division and function in brown and beige adipocytes. (A) Transmission EM analysis of BAT from control and *Pex16-AKO* mice kept at room temperature or subjected to cold exposure. Peroxisomes (black dots) were detected by staining using 3, 3'-diaminobenzadine (DAB). Notice the difference in mitochondrial morphology between the genotypes at 4°C. Scale bar, 500 nm. (**B**) Aspect ratio (ratio of major axis length to minor axis length) measured in BAT mitochondria. The data are based on 15 mitochondria per condition. (**C**) Number of mitochondria per cell based on TEM images of BAT taken at 1000-2000x magnification. The data are average of 8 cells per condition. (**D-E**) Mitochondrial DNA

copy number normalized to nuclear DNA measured by qPCR in BAT and iWAT; for BAT, n=6 per genotype at 22ºC and 3 per genotype at 4ºC; for iWAT, n=4 per genotype under each condition. (**F**) Gene expression analysis in BAT of cold-treated mice; n=4-5. Data are expressed as mean±SEM. and were analyzed by one-way ANOVA followed by Fisher's least significant difference (LSD) test (panels B-E) or by Student's t-test (panel F); *P<0.05; **P<0.01; ***P<0.001.

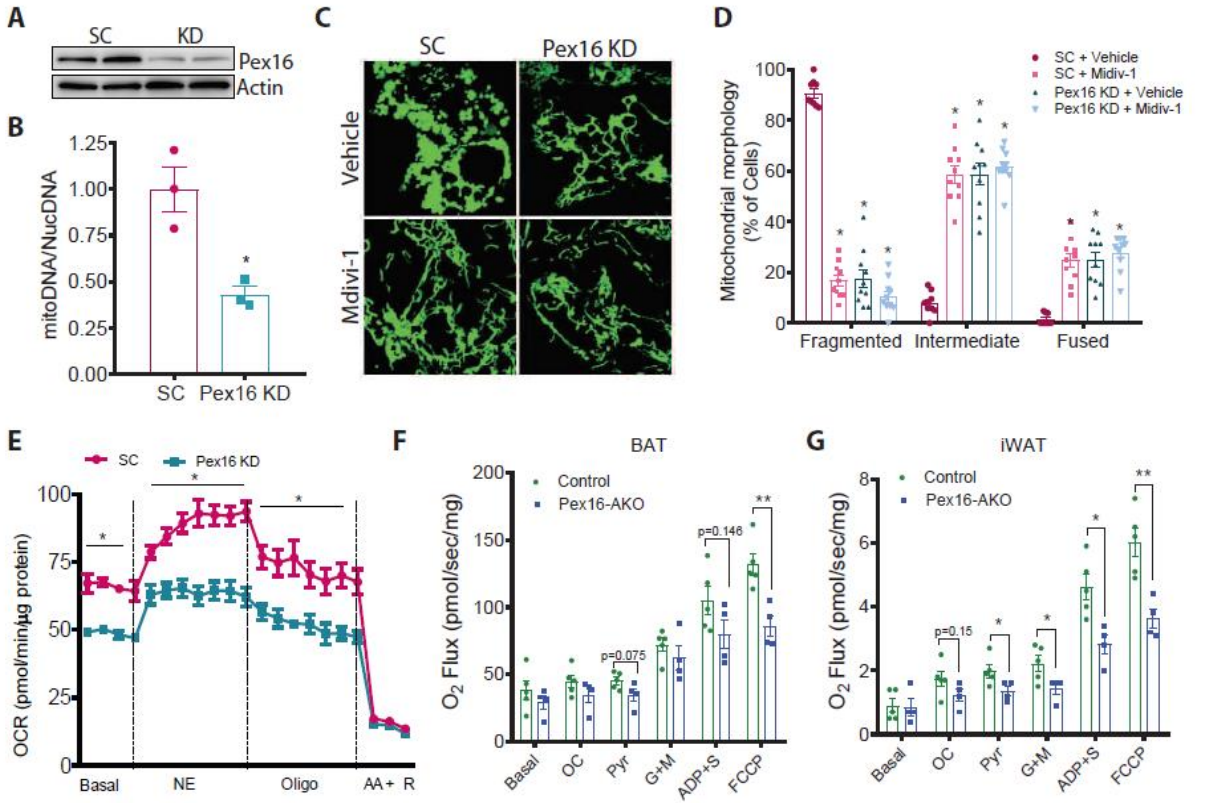

Figure 5. Cell autonomous effects of Pex16 inactivation on mitochondrial dynamics and function. (**A-B**) BAT SVF cells were subjected to brown adipogenesis for 4 days and then treated with scrambled or Pex16 shRNA and analyzed after additional 5 days using immunoblotting and mitochondrial DNA content measurement by qPCR. N=3 in panel B. (**C)** BAT SVF cells stably expressing lentiviral-encoded mito-GFP were differentiated into adipocytes and then treated with scrambled or Pex16 shRNA in the presence or absence of Mdivi-1 and analyzed 5 days later for mitochondrial morphology using confocal microscopy. Images are representative of 3 separate experiments. (**D)** Quantification of mitochondrial morphology of the cells in Panel C. (**E)** Effect of Pex16 knockdown on oxygen consumption rate measured in BAT SVF cells using a Seahorse XF24 Extracellular Flux Analyzer; n=5. (**F-G**) Measurement of mitochondrial respiration using an Oroboros Oxygraph system in permeabilized BAT and iWAT from control and *Pex16-AKO* mice following sequential additions of octanoyl-I-carnitine, OC; pyruvate, Pyr; glutamate and malate, G+M; adenosine diphosphate and succinate, ADP+ S; and FCCP; n=4-5. Data are expressed as mean±SEM. and were analyzed by Student's t-test; *P<0.05; **P<0.01.

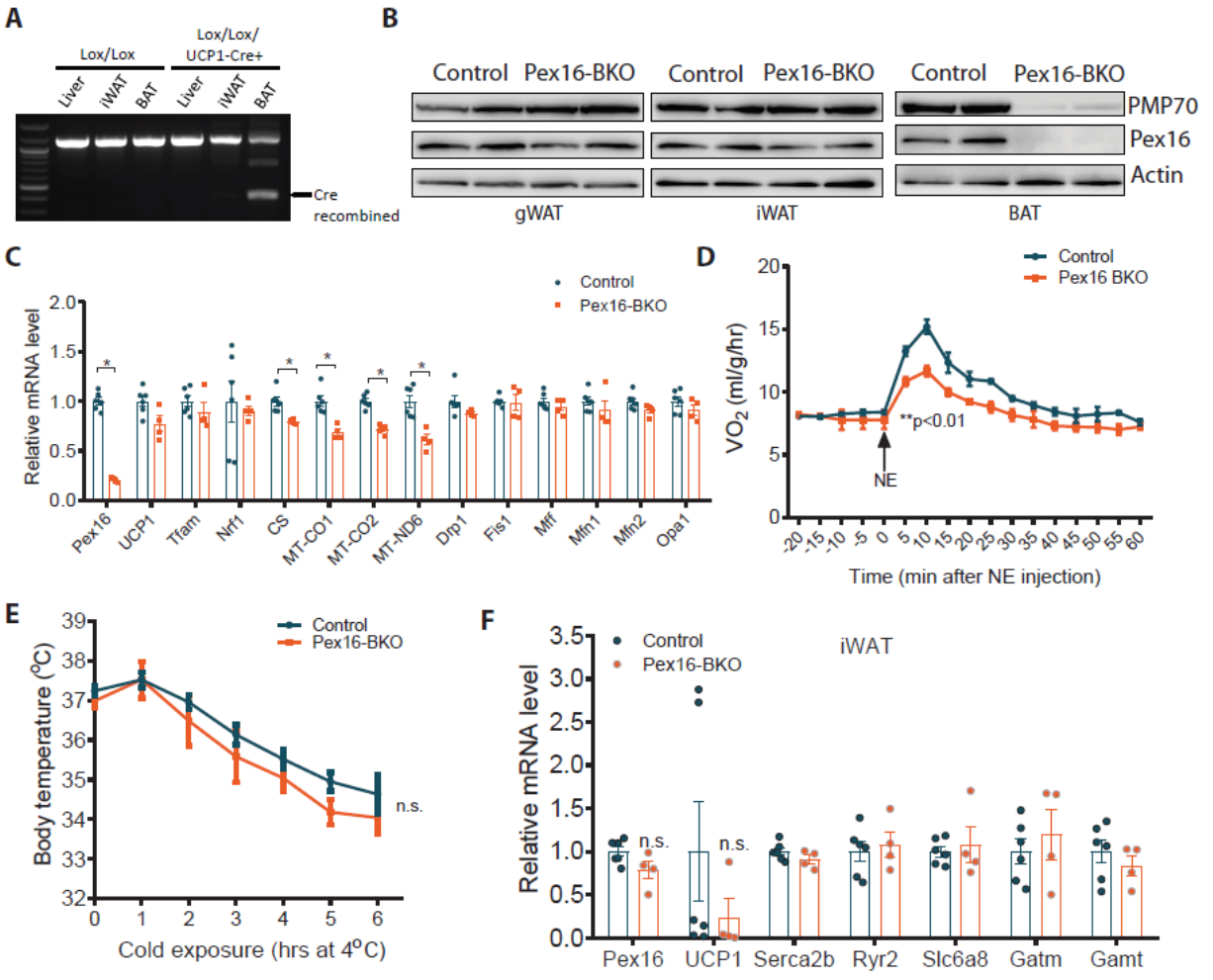

Figure 6. Generation and characterization of BAT-specific Pex16 knockout mice.(**A**) Analysis of Cre-mediated recombination by PCR. (**B**) Western blot analysis in BAT, iWAT and gWAT. (**C**) Gene expression analysis by quantitative real-time PCR in BAT; n=4-6. (**D**) Oxygen consumption rate (VO_2) measured in control and *Pex16-BKO* mice using indirect calorimetry before and after intraperitoneal NE injection; n=4. (**E**) Rectal temperature of control and *Pex16-BKO* mice subjected to a 6 hr cold challenge; n=5-6. (**F**) Quantitative real-time PCR analysis in iWAT of mice subjected to an overnight cold exposure, n=4-6. Data are expressed as mean±SEM and were analyzed by Student's t-test (panels C and F) or 2-way ANOVA with Bonferroni post test (panels D and E); *P<0.05; **p<0.01; n.s., not significant.

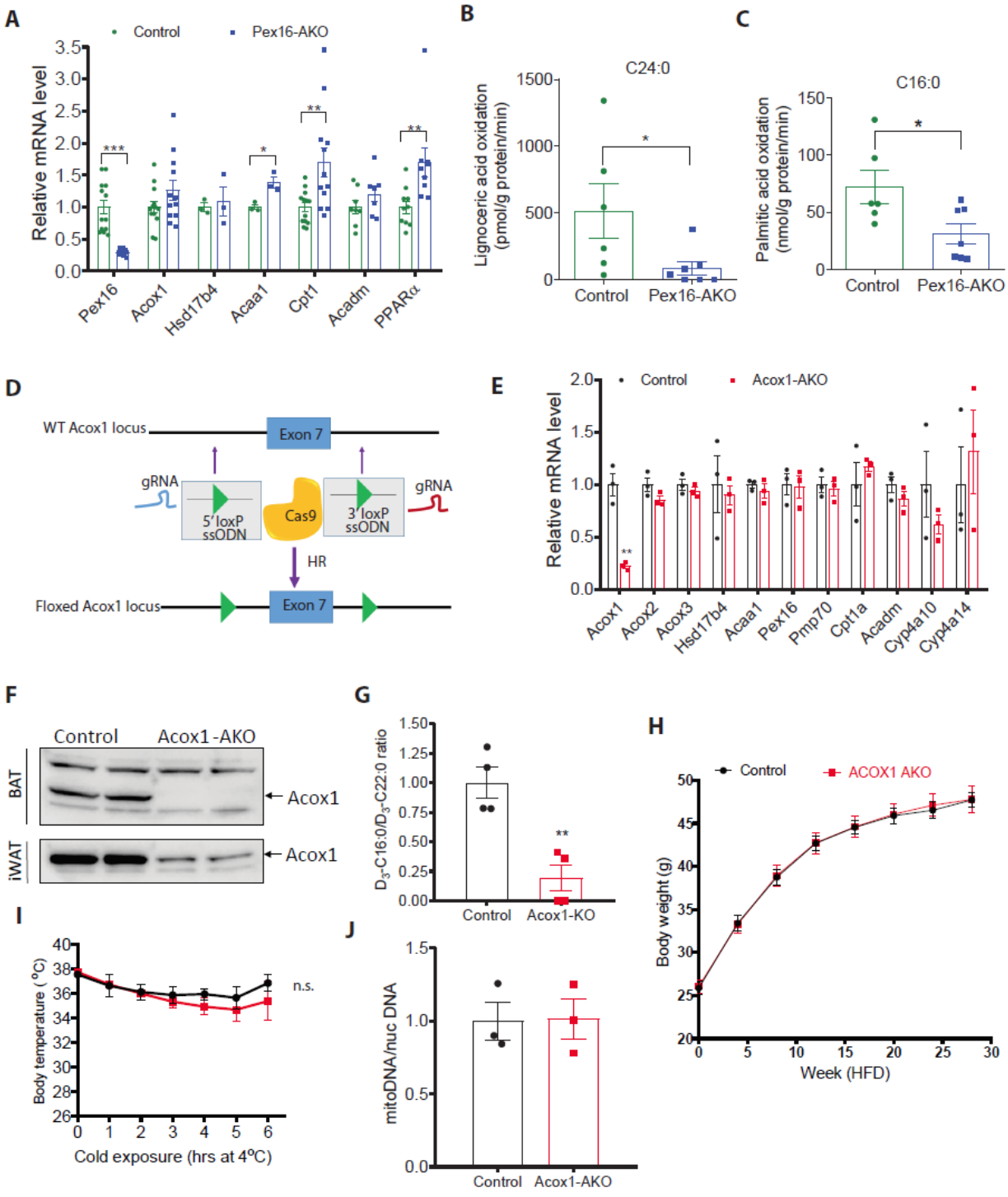

Figure 7. *Pex16-AKO* mice have impaired FAO, but adipose-specific inhibition of peroxisomal FAO is not sufficient to promote diet-induced obesity or impair thermogenesis. (**A**) mRNA levels of fatty acid oxidation genes in BAT of control and *Pex16-AKO* mice; n=3-13. (**B-C**) Beta oxidation of lignoceric acid (C24:0) and palmitic acid (C16:0) in BAT; n=6-7. (**D**) Gene targeting strategy using CRISPR/Cas9 to insert loxP sites into the Acox1 locus. The floxed

mice were crossed with an adiponectin-Cre mouse to generate *Acox1-AKO* mice. (**E**) qPCR analysis of fatty acid oxidation and peroxisomal biogenesis genes; n=3. (**F**) Western blot analysis of Acox1 knockout in BAT and iWAT. (**G**) Control and Acox1-KO iWAT SVF cells were incubated with D3-C22:0, whose catabolism to D3-C16:0 was measured mass spectrometrically. Fatty acid oxidation was expressed as ratio of D3-C16:0 to D3-C22:0; n=4. (**H**) Body weight of control and *Acox1-AKO* mice fed a HFD and maintained at normal room temperature; n=13-18. (**I**) Cold tolerance was determined by measuring rectal temperature at the indicated times after cold exposure; n=4-5. (**J**) Mitochondrial DNA content normalized to nuclear DNA in BAT of control and *Acox1-AKO* mice subjected to cold exposure; n=3. Data are expressed as mean±SEM. Student's t-test was used for analysis of the data in panels A-C, E, G and J were analyzed by Student's t-test. Two-way ANOVA with Bonferroni post test was used for analysis of the data in panels I. *P<0.05; **P<0.01; **P<0.001; n.s., not significant.

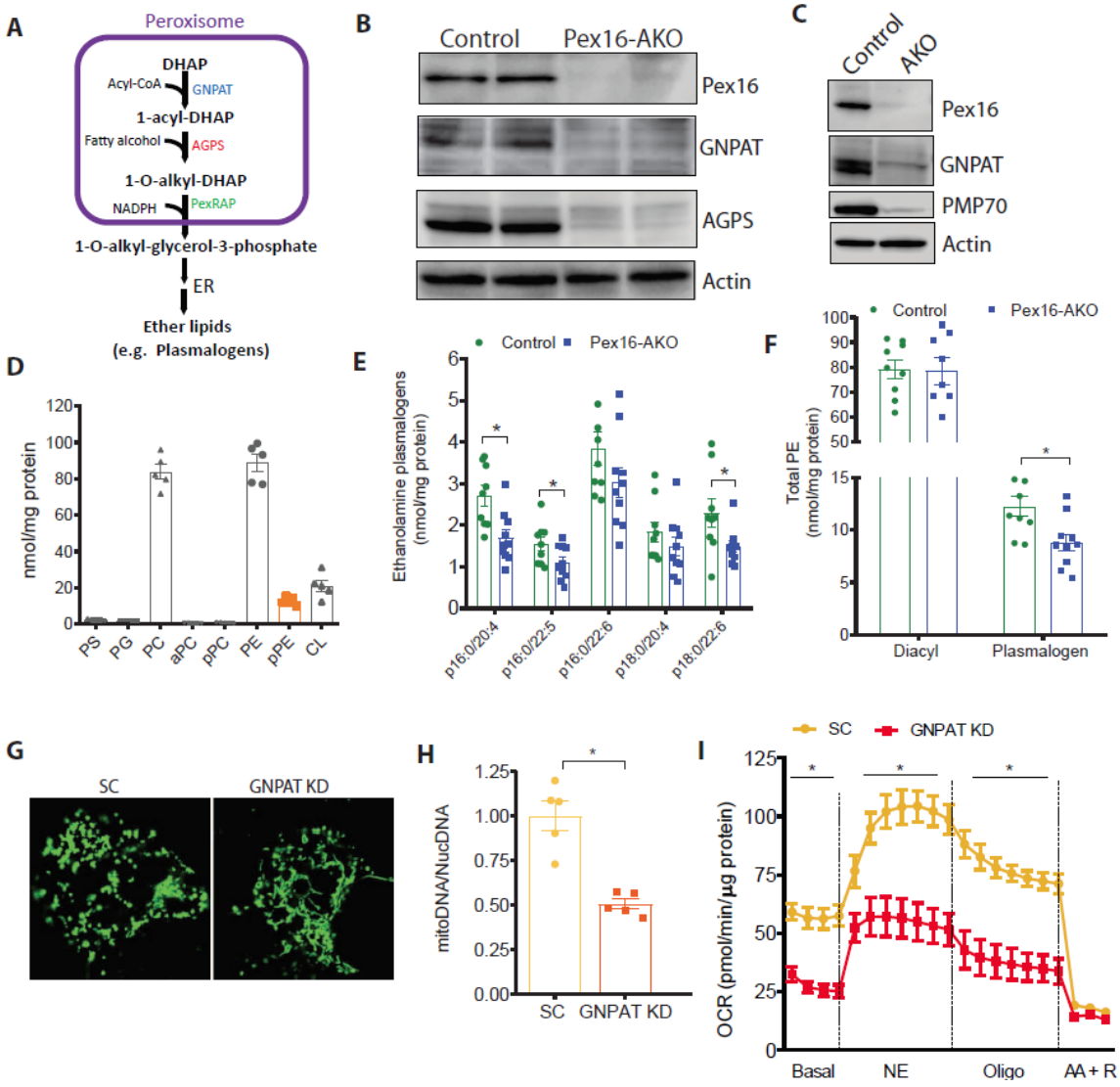

Figure 8. Peroxisome-derived lipids are present in mitochondria and inhibition of their synthesis reduces mtDNA content and impairs mitochondrial function. (**A**) Ether lipid synthetic pathway. The initial steps for synthesis of ether lipids, including plasmalogens, take place in peroxisomes, generating 1-O-alkyl-glycerol-3-phosphate (AGP), a precursor for ether-linked analogs of phosphatidylcholine and phosphatidylethanolamine. (**B-C**) Western blot analysis suggesting that ether lipid synthetic enzymes are degraded in BAT (**B**) and iWAT (**C**) of *Pex16-AKO* mice (**D**) Targeted lipidomics analysis of mitochondrial phospholipids in BAT of wild-type C57 mice. PS, phosphatidylserine; PG, phosphatidylglycerol; PC, phosphatidylcholine; aPC, alkyl ether PC; pPC, plasmalogen PC; PE, phosphatidylethanolamine; pPE, plasmalogen PE; CL, cardiolipin; n=5. (**E**) Levels of various plasmalogen PE species in the mitochondrial fraction of BAT; n=9-10. (**F**) Total diacyl and plamalogen PE content in BAT mitochondria. (**G**) BAT SVF cells stably expressing lentiviral-encoded mito-GFP were differentiated into adipocytes and then treated with scrambled or GNPAT shRNA and analyzed 5 days later for mitochondrial morphology

using confocal microscopy. Images are representative of 3 separate experiments. (**H**) Differentiated BAT SVF cells were treated with scrambled or GNPAT shRNA. Five days later, mtDNA copy number normalized to nuclear DNA was measured by qPCR; n=5. (**I**) Effect of shRNA-mediated knockdown of GNPAT on oxygen consumption rate was measured in BAT SVF cells using a Seahorse XF24 Extracellular Flux Analyzer; n=8. Data are expressed as mean±SEM and were analyzed by Student's t-test. *$P<0.05$.

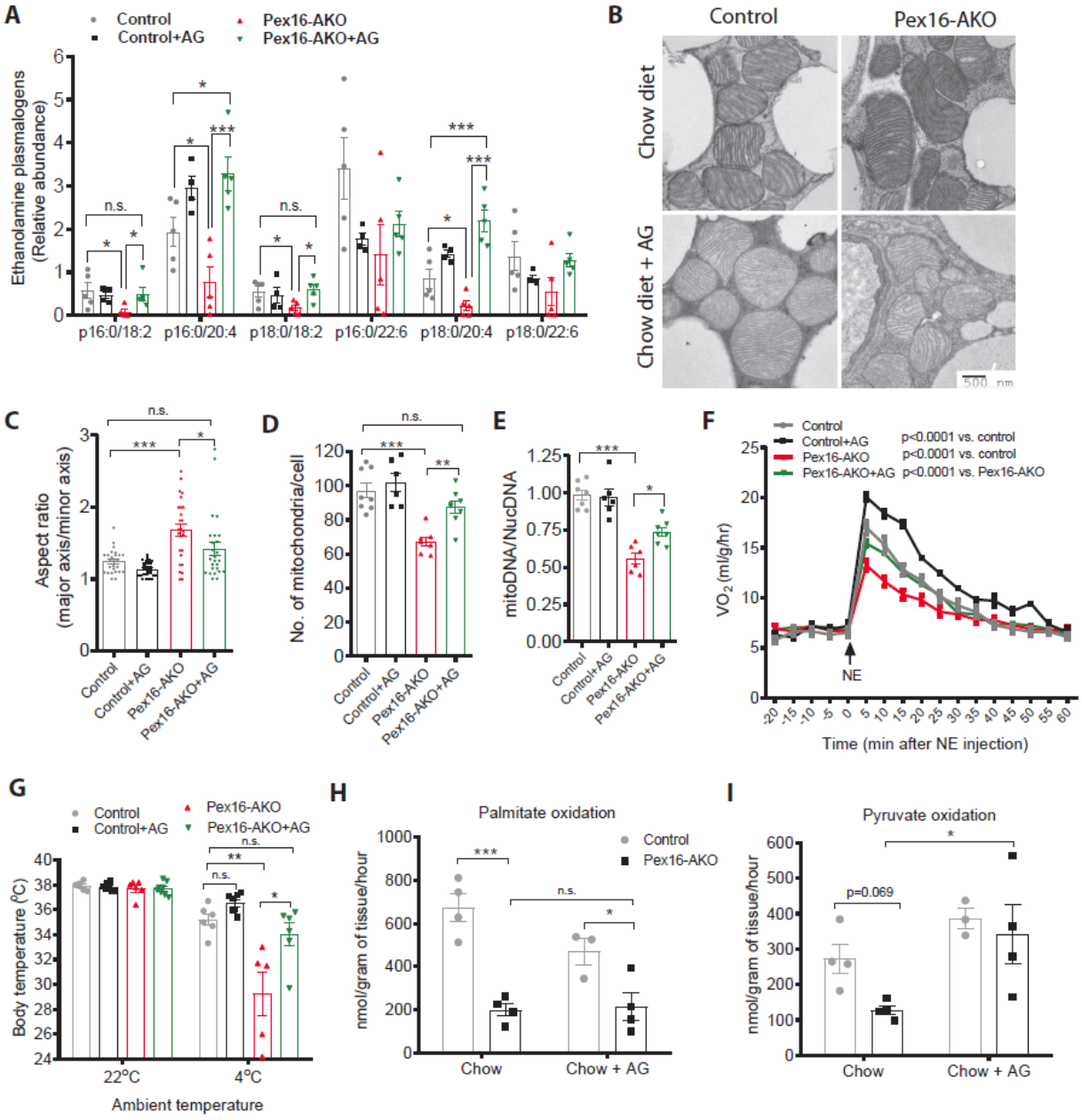

Figure 9. **Dietary supplementation of plasmalogens rescues mitochondrial morphology and function and improves cold tolerance in *Pex16-AKO* mice.** (**A**) Mass spectrometric analysis of PE plasmalogens in the mitochondrial fractions from control and *Pex16-AKO* mice treated with or without alkylglycerol (AG) for 8 weeks; n=5. (**B**) TEM analysis of mitochondrial morphology in BAT of control and *Pex16-AKO* treated with or without AG, followed by cold exposure. (**C**) Aspect ratio measured in BAT mitochondria from control and *Pex16-AKO* mice. The data are based on 26 mitochondria per condition. (**D**) Number of mitochondria per cell based on TEM images of BAT taken at 1000-2000x magnification. The data are average of 6-8 cells per condition. (**E**) mtDNA measured by PCR in BAT of control and *Pex16-AKO* mice treated with or without AG, followed by cold exposure; n=6-7. (**F**) VO_2 was measured using indirect calorimetry before

and after intraperitoneal norepinephrine (NE) injection; n= 8-9. (**G**). Cold tolerance was determined by measuring rectal temperature prior to and after 6 hrs of cold exposure; n=6-8. (**H-I**) Fatty acid and pyruvate oxidation assays in BAT; n=3-4. Data are expressed as mean±SEM and were analyzed by one-way ANOVA, followed by Fisher's LSD test (panels A, C-E and G-I), or two-way ANOVA with Bonferroni post test (panel F); *$p<0.05$; **$p<0.01$; ***$p<0.001$; n.s., not significant.